Master Thesis

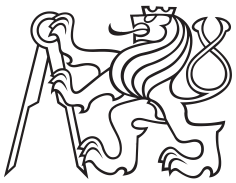

Czech Technical University in Prague

F3

Faculty of Electrical Engineering
Department of Measurement

Universal flight computer for a student rocket

Bc. Lukáš Mičan

Supervisor: Ing. David Novotný
May 2024

MASTER‘S THESIS ASSIGNMENT

I. Personal and study details

Student's name: **Mičan Lukáš** Personal ID number: **487005**

Faculty / Institute: **Faculty of Electrical Engineering**

Department / Institute: **Department of Measurement**

Study program: **Cybernetics and Robotics**

II. Master’s thesis details

Master’s thesis title in English:

Universal flight computer for a student rocket

Master’s thesis title in Czech:

Univerzální letový počítač pro studentskou raketu

Guidelines:

Design, realize and test a platform for universal flight computer for a student rocket. The flight computer should include a basic set of sensors required for flight. (e.g. barometer, accelerometer and GPS receiver). Additionally the computer should be able to process input data from multiple sensors (voltage measurement in range of external sensors, current loop signal 4-20mA) and control outputs (power output for resistive load, PWM control of motors and servos, continuityt testing). The computer should be able to communicate with other electronic components of the rocket using RS485/CAN interface and with the ground station via wireless connection. The flight data records should be stored in EEPROM memory or SD card.

Bibliography / sources:

[1] Vít Záhlava: Návrh a konstrukce DPS, Ben 2010
[2] VEDRAL, Josef a Jan FISCHER. Elektronické obvody pro měřící techniku. Vyd. 2. Praha: Vydavatelství ČVUT, 2004. ISBN80-01-02966-2.
[3] TI application Note: A Basic Guide to Bridge Measurements, 2022, available at: https://www.ti.com/lit/an/sbaa532/sbaa532.pdf

Name and workplace of master’s thesis supervisor:

Ing. David Novotný Department of Measurement FEE

Name and workplace of second master’s thesis supervisor or consultant:

Date of master’s thesis assignment: **03.02.2023** Deadline for master's thesis submission: _____

Assignment valid until:
by the end of summer semester 2024/2025

Ing. David Novotný Supervisor’s signature	Head of department’s signature	prof. Mgr. Petr Páta, Ph.D. Dean’s signature

III. Assignment receipt

The student acknowledges that the master’s thesis is an individual work. The student must produce his thesis without the assistance of others, with the exception of provided consultations. Within the master’s thesis, the author must state the names of consultants and include a list of references.

Date of assignment receipt	Student’s signature

Acknowledgements

I would like to thank to my thesis advisor, Ing. David Novotný, for his calm guiding during the preparation of this thesis.

I would also like to express my gratitude to the CTU Space Research team for the opportunity to work on this project as well as for providing all necessary technical equipment and tools required for realization of this project.

Last but not least I would like to thank Aleš Zapadlo for his valuable feedback.

Declaration

I declare that the presented work was developed independently and that all used sources of information used within this work are listed conforming to the Methodological guideline on observance of ethical principles in the preparation of university theses.

In Prague, on 24th May 2024

Abstract

With recent developments in space flight industry, rocketry is gaining popularity even among students and hobbyists. Many technical universities have established student teams focused on development of high-power rockets and space technologies. International rocketry competitions are being held in all parts of the world.

In this thesis, universal avionics platform for high-power rocket control is proposed. The design is focused on versatility to accommodate various requirements of different types of rockets. For this reason a modular approach is used. Safety of the whole system is considered as well. The design is based on requirements of CTU Space Research student team.

In addition, critical parts of the avionics platform such as the flight computer and section management board are designed, realized and tested in this thesis. These parts are designed to facilitate control of complex rockets using hybrid or liquid fuel engine as well as smaller model rockets.

Keywords:

rocket, flight computer, STM32, avionics, COTS, modular

Supervisor:

Ing. David Novotný
Department of Measurement, FEE

Abstrakt

Díky nedávnému vývoji v oblasti vesmírných letů, získává raketová technika na popularitě i mezi studenty a modeláři. Mnoho technických univerzit založilo studentské týmy zaměřené na vývoj vysoce výkonných raket a kosmických technologií. Mezinárodní raketové soutěže se konají ve všech částech světa.

V této práci je navržena univerzální avionická platforma pro řízení vysoce výkonných raket. Návrh je zaměřen na univerzálnost, aby vyhovoval požadavkům různých typů raket. Z tohoto důvodu je použit modulární přístup. Zohledněna je rovněž bezpečnost celého systému. Návrh vychází z požadavků studentského týmu CTU Space Research.

Kritické části avionické platformy, jako je letový počítač a deska pro ovládání částí rakety, jsou v této práci navrženy, zrealizovány a otestovány. Tyto části jsou navrženy tak, aby umožnili řízení složitějších raket využívajících motory na hybridní nebo kapalné palivo jakožto i menších modelářských raket.

Klíčová slova:

raketa, letový počítač, STM32, avionika, COTS, modulární

Překlad názvu:

Univerzální letový počítač pro studentskou raketu

Contents

Figures

Tables

Chapter 1

Introduction

Rocketry and spaceflight is gaining popularity with every year. With many significant advancements in the space industry, like reusable rockets and more efficient engines, the cost of spaceflight is at all time low and the demand for transportation of satellites to orbit is high. Many new companies have started development of their own rockets aiming to fill the demand for launching satellites. There are plans for sending man to the moon in the near future and establishing a space station there. The cost of satellite development and manufacturing is decreasing as well due to new technologies, new form factors and increased competition with multiple new companies entering this field.

This field is popular with students and hobbyists alike. Technical universities throughout Europe and America have established student teams focused on development of high-power rockets and satellites. These teams are an opportunity for students to try out their newly acquired skills and capabilities in a real project with hands-on experience. Student developed rockets can compete in many competitions around the world. This field has a longer tradition in America than in Europe with many amateur rocketry groups but lately this tradition is growing in Europe as well. In 2020, the European Rocketry Challenge was founded where student teams from european technical universities can participate. The teams develop high-power rockets aiming at target apogee of $3\,km$ or $9\,km$ with more complex systems including hybrid or liquid-fuel engines. In 2021, the Czech Rocket Challenge competition was founded in Czech Republic as well but this competition is intended for smaller groups and younger students instead. The rockets for this competition are smaller and simpler with ascent up to $1\,km$.

Onboard avionics are essential for a successful flight of a rocket. The flight computer needs to be able to detect important events like launch of the rocket, apogee of the flight path or touchdown of the rocket in order to control the actuators correctly. It is responsible for activation of the recovery system or opening and closing of valves at the correct moment. It needs to have the ability to sense and process data from multiple different sensors and to control the actuators used in the rocket. It needs to be robust and reliable in order to ensure correct operation in high vibration and high acceleration environment inside the rocket. Last but not least it needs to be able to communicate with a ground station to provide telemetry and control of the rocket.

In this thesis a system architecture of onboard avionics for a high-power or a model rocket is proposed and a flight computer is designed. The design is based on the requirements of the student team CTU Space Research for the Illustria rocket. The Illustria rocket is using a hybrid-fuel engine and thus the flight computer needs to be able to control valves and process pressure and temperature signals from sensors. Additionally the flight computer should be able to control smaller and simpler rockets as it may be used in the Vanguard rocket developed by CTU Space Research or rockets for the Czech Rocket Challenge competition.

The first part of the thesis discusses the requirements for onboard avionics and a new system architecture is proposed. In the second part the design of the proposed flight computer is described in detail including sensor selection process and power management. The third part describes the design of section management board used for interaction with actuators and sensors in a modular manner. Tha last part is focused on testing of the subsystems of the proposed flight computer.

Chapter 2

Rocket Onboard Avionics

The rocket onboard avionics is responsible for controlling the entire rocket. That includes multiple different tasks such as: position, velocity and attitude estimation, valve control, parachute deployment or active flight control.

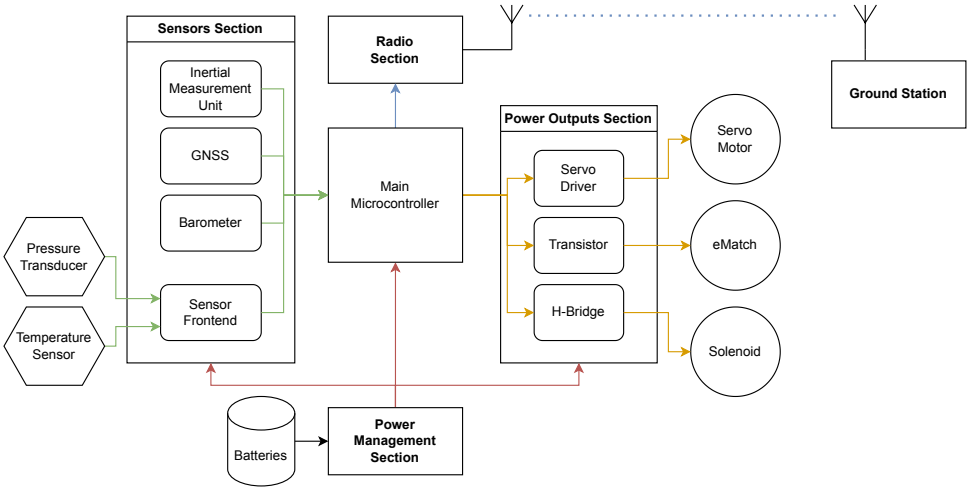

Figure 2.1: General high-power rocket avionics structure example

The onboard avionics for high-power or model rockets can be split into different sections by function as demonstrated in the figure 2.1. The sensor section measures required data from internal or external sensors and passes them to the main microcontroller for processing. The sensors usually include inertial measurement unit, global navigation satellite system (GNSS) receiver and barometer sensor as these are used for position estimation and detection of liftoff, apogee and touchdown. Additionally some external sensors can be required in more complex rockets, for example oxidizer tank pressure and temperature sensors in rockets with hybrid fuel engines.

Based on the processed data, the microcontroller commands power outputs section to perform different actions with actuators. The most important output is usually parachute deployment as it is responsible for safe landing of the rocket, but other devices such as servomotor or solenoid need to be controlled in more complex rockets for active flight control or valve actuation. The radio section is responsible for wireless communication between

the flight computer and the ground station. This includes transmission of flight telemetry data and rocket state information to the ground station and reception of commands from the ground station. Last but not least the power management section is responsible for power distribution to all parts of the onboard avionics.

2.1 Requirements

The flight computer designed in this thesis is based on the requirements of the student team CTU Space Research. It will be used in rockets developed by the team and thus it has to be able to cooperate with already existing parts as well as with new parts that can be developed in the future. The aim of this project is to design a flight computer as universal as possible to allow for easy expansion of the rocket without the need to completely redesign the onboard avionics.

2.1.1 Illustria Rocket

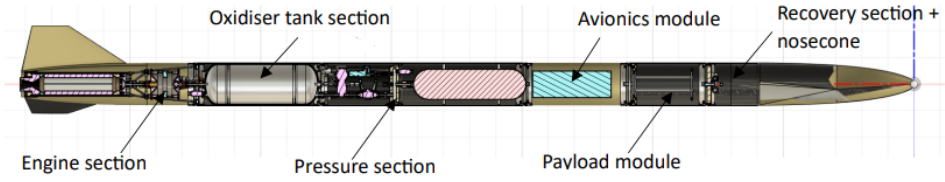

Figure 2.2: Scheme of the Illustria rocket

The Illustria rocket is the main project of CTU Space Research and it is designed for the European Rocketry Challenge competition. It is a 3.54 m tall rocket with outer diameter of 161 mm. It features modular design consisting of 6 sections as can be seen in figure 2.2. The modular design allows for easy change of the rocket sections which can be useful for incremental development as any section can be modified without the need to rebuild the whole rocket again. Moreover the modularity makes it possible to use different types of engines with the same avionics, payload and recovery sections. In addition it simplifies assembly before launch and allows for easier transportation. With total launch mass of 29 kg and maximum engine thrust of 1.9 kN, Illustria can reach maximum acceleration of 80 m/s^2 and maximum velocity of 260 m/s in order to achieve the target apogee of 3 km. It is able to carry a payload in form of a 2U CubeSat with mass of 2 kg. In the future an apogee of 9 km will be targeted.

The rocket is powered by a student researched and developed (SRAD) hybrid fuel engine burning ABS plastic as a solid fuel with nitrous oxide (N_2O) as a liquid oxidizer. Since the engine uses liquid oxidizer and an additional nitrogen gas (N_2) pressurizer, the flight computer needs to be able to control several valves and process pressure and temperature signals

from sensors to ensure correct operation of the rocket systems. The flight computer is responsible for control of the oxidizer tanking process as well as the launch procedure. The propulsion system is equipped with two valves operated by servomotors and a main electromagnetic valve. The servomotors are controlled via a pulse-width modulated (PWM) signal but a switch to digitally controlled serial bus servomotors is planned in the future and the flight computer needs to be prepared for that. The electromagnetic valve is bistable and does not require a constant current to operate, however, it needs a high current pulse in range of $3 - 6\,A$ to open or close. The propulsion system uses industrial pressure transducers and temperature sensors with a $4-20\,mA$ current loop output. Optionally a platinum or NTC thermistor can be used for sensing the engine and oxidizer tank surface temperature. Engine ignition is controlled by an external ground support equipment and does not require any additional hardware components in the onboard avionics.

The recovery system ensures the safe return of the rocket to the ground and thus needs to be reliable. Recovery system in Illustria consists of two parachutes - drogue and main. The drogue parachute deploys after reaching the apogee and its purpose is to slow down the descend of the rocket. It is important that the drogue parachute does not slow down the descent too much to prevent the wind from blowing the rocket far away from the launch site. The main parachute deploys at predefined altitude above ground (usually around $500\,m$) and slows down the rocket descend to a safe landing speed. The flight computer is responsible for detecting those events and for activation of the recovery system accordingly. The parachutes are deployed using a pyrotechnic charge that is ignited by an electric match. An electric match is a resistive element that easily ignites when heated by an electric current [1]. Electric matches used in the Illustria rocket have resistance of $1\,\Omega$. They require a minimum current of $0.7\,A$ to ensure ignition and maximum current of $0.03\,A$ to avoid ignition. In addition a glow wire can be used for the recovery deployment in the future. The valves, sensors and electric matches are distributed throughout the entire rocket and the design of the flight computer needs to respect this.

To detect events such as apogee and altitude above ground a set of sensors is required. A barometer is widely used in commercial solutions for this purpose as it does not need any advanced data processing and works reliably. Additionally an inertial measurement unit is useful for future development of the rocket as it allows for trajectory estimation and active control. Furthermore a GNSS receiver greatly helps with rocket recovery after landing and aids with the trajectory estimation.

The flight computer is required to have the ability to communicate with the ground station to provide rocket status data and remote control of the actuators. The internal valves in the rocket need to be operated according to the commands from mission control during tanking procedure and pre-flight checks. This can be done using radio communication or by a detachable cable, however, the flight computer needs to be able to send the flight telemetry data wirelessly during and after the flight as well. The telemetry information

is tracked by the mission control staff to determine the state of the rocket and in case any issues arise they can abort the flight. On abort, the flight computer shuts down the engine if is it still burning and deploys parachutes to slow the rocket down as much as possible.

2.1.2 Vanguard Rocket

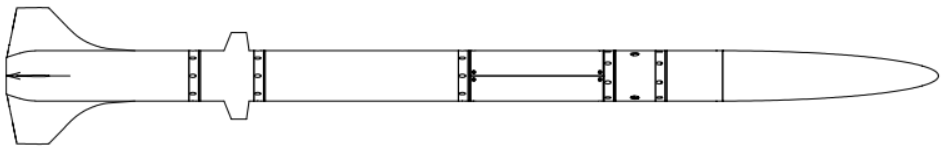

Figure 2.3: Scheme of the Vanguard rocket

The Vanguard rocket is a smaller rocket developed by CTU Space Research. It is 1.61 m tall with 94 mm in diameter and uses a modular construction similarly to the Illustria rocket. It is intended as a testing and verification platform for new technologies such as active flight control or new recovery systems. Flight computer software and algorithms can be tested there as well. This helps to ensure only mature parts are used in the larger Illustria rocket where unreliable or insufficiently tested parts can become a dangerous and expensive problem.

The rocket is powered by a SRAD solid fuel engine burning a mixture of sorbitol as fuel and potassium nitrate (KNO_3) as an oxidizer, more commonly known as "rocket candy" [2]. Since the solid fuel engine is much simpler than hybrid fuel engine, it does not require any special sensors or actuators. At launch it is ignited by an external ground support equipment. The engine can accelerate the rocket up to 190 m/s with thrust of 400 N and can reach apogee of 1 km. The maximum expected acceleration is 63 m/s^2 with launch mass of 6 kg.

Similarly to Illustria, the recovery system consists of two parachutes deployed by a pyrotechnic charge. The onboard sensors for recovery events detection and trajectory estimation are required as well as the wireless telemetry connection. A notable difference is the inclusion of active roll control section that is being developed by CTU Space Research. In future this section will be expanded to allow full flight control and the design of the onboard avionics should be prepared for that. New recovery systems may be tested on this rocket as well.

2.1.3 Rocket for Czech Rocket Challenge

Another use-case for the flight computer is a rocket for the Czech Rocket Challenge competition. The competition is aimed at high school or university student teams designing their own small model rockets. The competition

organizers provide all participants with the same solid-fuel engine which is the main constraint of the rocket design. The 43.4 mm outer diameter of the engine limits the minimal rocket diameter and exactly defined thrust curve with maximum thrust of 65 N forces the designers to find a compromise between rocket mass and maximum reached apogee.

Similarly to previously described rockets the flight computer is required to detect flight stages and to correctly deploy the recovery system. The rocket can employ various different recovery systems but usually they are actuated by a pyrotechnic charge, a glow wire, a servomotor or a solenoid. Optional tasks for the participants include active roll control or ground station development. This requires the ability of the flight computer to drive a servomotor and to communicate wirelessly for telemetry transmission.

2.1.4 Software

The flight computer is required to be able to run flight software already developed by the CTU Space Research team with minimal modifications as it has been flight proven. It is a bare-metal microcontroller firmware implementation with a simple in-house developed scheduler. The current flight computer software has been developed in the STM32CubeIDE using its hardware abstraction layer, thus the flight computer shall use a STM32 microcontroller.

In addition the team intends to switch to the PX4 system in the near future. It is a real-time operating system (RTOS) based on the NuttX system that is widely used in drones and other unmanned aerial vehicles [3]. This will simplify the development of the flight software thanks to the fact that many of basic features needed for more complex projects have already been implemented in the operating system and do not need to be re-implemented. For example threads, queues, scheduler, communication between threads or synchronization primitives are already working well in the RTOS. Furthermore a lot of other support software for this system is already available helping with development, testing, control and monitoring of the flight computer.

An optional feature is the ability to run Matlab generated software. This is an experimental way of flight software development that the CTU Space Research team wants to try out. It allows development of flight software in Matlab environment that is widely used in academic community and in control engineering especially. The developers can use advanced data processing and control algorithms present in Matlab and its toolboxes as well as a graphical programming with Simulink software.

2.2 Commercial and Alternative Solutions

Many commercial solutions for this task are available on the market. They differ wildly in the complexity of the design, size, cost and abilities. Large amount of the available legacy solutions are based on 8-bit microcontrollers

with only a barometer sensor and a power output for recovery system deployment. These represent a minimal flight computer for the simplest rockets. However, new and more advanced solutions are becoming available. The flight computers are gradually switching to 32-bit microcontrollers to allow for more advanced data processing and control algorithms. They include more sensor types such as accelerometer, gyroscope or magnetometer as well as global navigation satellite system receivers and integrated wireless transmitters. Many of them contain multiple outputs for pyrotechnic charges or servomotors. Few of the available flight computers were selected as a reference for comparison with the flight computer designed in this thesis. The legacy 8-bit flight computers were intentionally left out of the comparison as they offer minimal features compared to their modern counterparts. Many amateur projects based on Arduino development boards are also available but these were left out as well due to often missing technical specifications or incomplete design.

CATS Vega

The CATS Vega is an advanced flight computer equipped with 32-bit microcontroller. Inertial measurement unit, barometer sensor, GNSS receiver, telemetry transceiver and a buzzer are present on the flight computer. It is capable of driving two pyrotechnic charges and two servomotors. Flash memory is used for storing flight data. USB-C is used for configuration and data download. [4] In addition, it is a mandatory secondary flight computer on the EuRoC competition used for unified apogee measurement.

BPS.Space Signal R2

BPS.Space Signal R2 is another example of advanced flight computer. It features a 32-bit microcontroller, inertial measurement unit, barometer sensor and a buzzer. It is capable of driving three pyrotechnic charges and two servomotors. Flash memory and microSD card are used for storing flight data. Bluetooth is used for configuration. [5]

Eggtimer Quasar

Eggtimer Quasar features a 32-bit microcontroller, barometer sensor, buzzer, GNSS receiver and telemetry transceiver. Three power outputs capable of driving pyrotechnic charges or servos are available. Storage for flight data logging is provided. WiFi is used for configuration and data download. [6]

Silicdyne Fluctus

Silicdyne Fluctus features barometer, 200G accelerometer, gyroscope, temperature sensor, buzzer, GNSS receiver and telemetry transceiver. It is capable of driving three pyrotechnic charges and four servomotors. In contrast with other flight computers, two analog inputs are also available. Flash memory

is used for storing flight data. MicroUSB is used for configuration and data download. [8]

Cimrman Mini 2

Cimrman Mini 2 is flight computer developed by CTU Space Research. It is aimed at smaller rockets, but an expander board was designed to allow control of rockets with hybrid fuel engine. It uses 32-bit microcontroller along with 64G accelerometer, gyroscope, barometer, magnetometer, buzzer and telemetry transceiver. On its own, it is capable of driving one pyrotechnic charge and one servomotor. EEPROM memory is used for storing flight data. USB-C is used for configuration. [7]

2.3 Proposed System Architecture

The proposed avionics system architecture focuses on versatility and reliability. Safety of the whole system was also considered, because the flight computer can interact with dangerous parts such as pyrotechnic charges or valves operating at high pressures. The onboard avionics aims to cover requirements of multiple different types of rockets as described in paragraph 2.1.

2.3.1 System Overview

Modular Approach

Modular approach was selected for the whole onboard avionics system. This simplifies the use in modular rockets such as the Illustria or Vanguard thanks to much simpler wiring, compared to a centralized design where each cable has to be wired all the way to the main flight computer. With modular design only a single cable harness with a single connector is needed to connect the different modules. In addition, the sensors and actuators can stay connected to the section management board in each section in the event of partial rocket disassembly. Therefore assembly and disassembly is a matter of just connecting or disconnecting a single connector at each section. This is very helpful when preparing the rocket for a flight. Prior to the launch, the rocket is partially assembled and prepared in the team workshop where all equipment is readily available. At the launch site the rocket is fully assembled for the flight with limited equipment and time. The modular design simplifies this process and saves time required for assembly.

Another advantage of modular design is that the onboard avionics can be easily modified to accommodate different types of rockets. The onboard avionics can be configured to support multiple sensors or actuators by just adding or removing the section management boards. This allows using the same control software for different types of rockets with just a modification of the software configuration. Furthermore, multiple people can be involved in the development of the onboard avionics system thanks to clear separation

of tasks either in hardware and software. In larger rockets such as Illustria, modularity allows for easier repair in case of any issues as the affected board can be just swapped out with a new one.

System Architecture

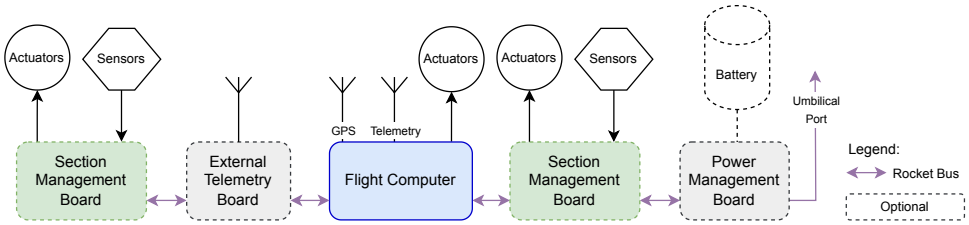

Figure 2.4: Possible system structure of the onboard avionics

The main parts of the onboard avionics are the main flight computer (FC) with codename "Cimrman 2" and the section management board (SMB) with codename "Zora 2". The codenames were selected according to existing naming conventions of the CTU Space Research team. A general possible system structure of the onboard avionics is shown in figure 2.4.

The flight computer is the main processing unit of the onboard avionics containing a set of sensors such as inertial measurement unit, barometer, magnetometer and GNSS receiver. It also contains a telemetry module for communication with the ground station. Additionally, it is equipped with two power outputs with continuity detection and a servomotor output for operating the actuators in simpler rockets. An onboard buzzer can be used for state indication or to help finding the rocket during recovery after landing.

The section management board is responsible for controlling parts in each rocket section and houses circuits for interfacing with sensors and actuators. It is able to monitor 4 sensors with $4 - 20\,mA$ current loop output or voltage output in range of $0 - 3.3\,V$. It is also able to control 4 servo outputs with PWM signal or single-wire UART signal. Four power outputs capable of delivering $6\,A$ with software-controlled polarity and continuity detection are available on the section management board and they can be used for e-match ignition or solenoid control. Last but not least the section management board contains a set of supercapacitors acting as a power backup for the onboard avionics and as a high current source for the servomotors or power outputs in order to minimize stress on the batteries, cables and connectors.

All parts of the avionics system communicate via Controller Area Network (CAN) bus. The CAN bus was selected for its features provided by the data link layer such as message priority and checksum support. [9] The message priority combined with carrier-sense multiple access with collision avoidance (CSMA/CA) is an important feature to ensure reliable communication between the flight computer and section management boards for mission critical events. For example a message to deploy the recovery system is much more important than a message with battery status. In addition the checksum

feature ensures correct reception of the messages. The publisher-subscriber model of communication is useful as well because the ground support equipment can monitor sensor status or operate valves directly when the rocket is on the launchpad. The differential pair physical layer helps to suppress common mode interference coupled onto the bus wires.

Power for all parts of the avionics system is delivered through a $11.4\,V$ high power line and a $5\,V$ stand-by power line. The separation of the two power lines allows safe operation during the disarmed state as described in paragraph 2.3.2. The high power line is intended for supplying the power outputs and servomotors when the rocket is armed, while the stand-by power line supplies the logic circuitry to allow communication with the flight computer in disarmed state. The combination of the two power lines and CAN bus in a single connector is internally called "Rocket Bus". Each part of the avionics system shall contain two Rocket Bus connectors to allow daisy-chaining of all parts. This is to ensure simple connection of all parts eliminating the need for splitters or additional connectors and to optimize the topology of the CAN bus.

Additional modules can be added to the avionics system in the future. They need to support the Rocket Bus connection for power and communication. For example a power management board or external telemetry board can be added to the avionics system.

The Rocket Bus can be brought out of the rocket to act as a umbilical port. This can be used to simplify the communication between onboard avionics and the ground support equipment during the tanking process as the wireless communication has limited bandwidth and can be prone to interference. The direct connection to the ground support equipment allows direct measurement of internal propulsion system pressures and temperatures and allows more reliable control of the internal valves.

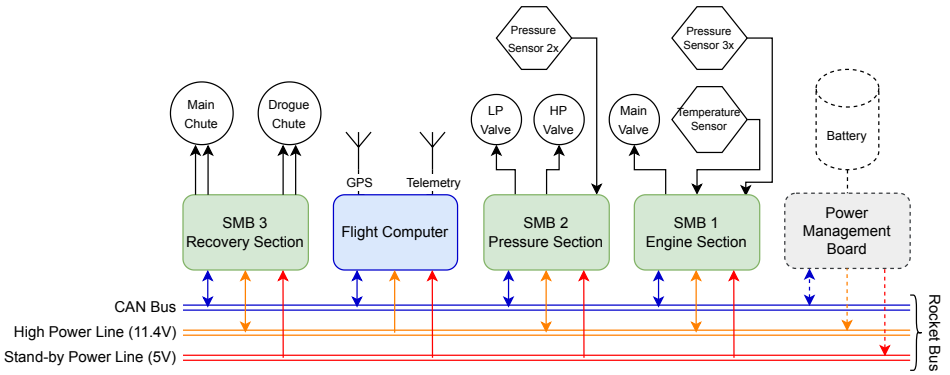

Figure 2.5: System structure for the Illustria rocket

Example system structure for the Illustria rocket is shown in figure 2.5. It uses multiple boards to facilitate control of all parts of the rocket, however, a simpler structure with just a flight computer can be used for the Vanguard rocket or rocket for the Czech Rocket Challenge competition as shown in figure 2.6.

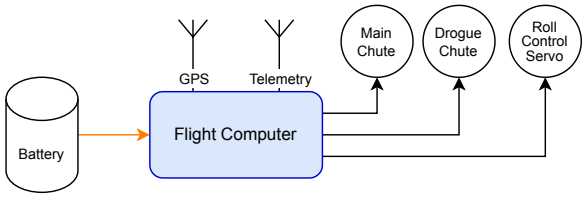

Figure 2.6: System structure for the Vanguard rocket

Connectors and cabling

The connectors used in the onboard avionics system are a critical component for reliability of the whole system. They need to withstand high vibration and stress while carrying high currents and vital communication data. Additionally they need to be small enough to fit well into the smaller rockets. A set of connectors was selected for use with all components of the onboard avionics as it ensures easy interoperability between different components in the rocket.

Among the wide variety of connectors available in the market, the Molex UltraFit connector series was selected for use with the Rocket Bus. It was found as the best fit for current rating, small size and reliability constrains. It is capable of supporting current up to $14\,A$ per pin with $3.5\,mm$ pitch using keyed and latched receptacles [10]. The connector terminals use 6 points of contact with gold plating to ensure reliable connection and higher current carrying rating. Terminal position assurance retainers are available to further improve reliability. For use with the Rocket Bus the dual row 6-pin variant was selected. The assigned pin functions are listed in table 2.1. The pin assignment order was selected to simplify trace routing on the PCB while keeping related pins close together to minimize impact of interference.

Pin Number	Name	Description
1	V_PWR	High power line positive (11.4V)
2	GND_STBY	Stand-by power line ground
3	V_STBY	Stand-by power line positive (5V)
4	GND_PWR	High power line ground
5	CAN+	CAN bus dominant high
6	CAN-	CAN bus dominant low

Table 2.1: RocketBus Connector Pin Assignment

For use with sensors and actuators the Molex KKPLUS 250 connector series was selected. It offers high current rating up to $6.5\,A$ per pin in small package with $2.5\,mm$ pitch [11]. The receptacles are latched for reliable connection in high vibration environment. In addition the receptacles are keyed to ensure correct connection of all components. The connectors use shrouded wall to improve durability of the connection and to protect against accidental short circuit of the exposed connector pins. This connector series was selected for connection of actuators, sensors and other expansion ports such as UART or I2C. Multiple pin count variants are used: 2 pin variant for the high power

output (e-matches, glow wires and solenoids), 3 pin variant for servomotors and sensors and 4 pin variant for UART and I2C. The assigned pin functions for servo and sensor connectors are listed in table 2.2 and 2.3.

Pin Number	Name	Description
1	GND	Servo ground
2	PWR	Servo power
3	SIG	Servo signal (PWM or single-wire UART)

Table 2.2: Servo Connector Pin Assignment

Pin Number	Name	Description
1	GND	Sensor ground
2	PWR	Sensor power
3	SIG	Sensor signal (current loop or voltage)

Table 2.3: Sensor Connector Assignment

The cables used in the rocket need to be carefully selected as well. In rockets with hybrid fuel engines there can be very low temperatures during the tanking process or during engine burn due to gas expansion, thus the cables need to withstand these temperatures without any issues. For that reason cables with radiation cross-linked ETFE insulation were selected as they provide increased resistance to tensile, shear and compressive forces [12] and can withstand temperatures between $-65\,°C$ and $150\,°C$ [13]. In addition the radiation cross-linked insulation of the cables can be thinner which is useful when the cable is routed through narrow airfoils.

2.3.2 Power Management

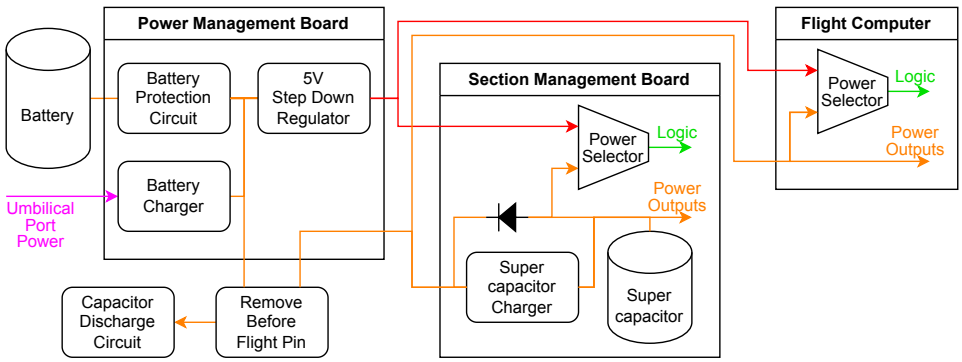

Figure 2.7: Power Management Scheme

The power management system is another crucial component of the onboard avionics system. It must be designed in such a way that it can deliver stable power to the avionics system during all flight stages in order for the flight to

be successful. The proposed power management and distribution system is described in figure 2.7.

The main power source is a Li-Ion battery pack. The Li-Ion chemistry was selected because of its higher power density compared to other types of batteries (NiCD, NiMH) and is easily available in a durable 18650 package. The Li-Po chemistry was banned from use at the EuRoC competition because it is often sold in less durable packages that could cause a fire after a rough landing of the rocket. Either two-cell (7.2V) or three cell (11.4V) battery packs can be used depending on voltage required for the actuators used in the rocket.

The main power source is split into a high power line and a stand-by power line. The stand-by power line is used for powering the logic circuits while the rocket is in disarmed state and its voltage can be between $4.5\,V$ and $13\,V$. The high power line is used for powering the actuators directly from the battery and must be connected through a switch in form of a remove before flight pin (RBFP). This helps to improve safety of the system because no actuators are powered up during the disarmed state, but it still allows communication with the flight computer for configuration and preflight preparation purposes.

Many actuator actions needed during the flight can be characterized as short ($< 2\,s$), high-current pulses, for example an e-match firing, a glow wire or solenoid activation or a servomotor movement from one position to another. Mission critical events such as recovery system deployment are dependant on these actions being performed successfully. For those reasons a secondary power reservoir in form of supercapacitors was introduced to support the high current pulses. The supercapacitors are charged using a charger circuit during the final preparations for the flight on the launchpad. They help to deliver the current needed during actuator activation in order to minimize stress on the batteries and to keep the power supply stable. In addition the supercapacitors act as a backup power supply in case of a power failure.

The supercapacitors are part of each section management board and can provide backup power to it. Moreover they can also provide backup power to all boards connected to the Rocket Bus. The section management boards are equipped with a reverse power delivery system in form of an ideal diode. The ideal diode is needed to allow slow charging of the supercapacitors avoiding overcurrent conditions while minimizing power loss during reverse power flow.

Each board is equipped with a power selector for powering the logic circuits. This helps to increase reliability of the system when the main power supply fails. The power selector automatically selects power source with the highest voltage and passes it to the logic circuits power regulator. The section management boards can use the supercapacitors as a backup power supply for logic circuits, but the flight computer can take advantage of the supercapacitors as well due to the reverse power delivery feature.

The onboard avionics system could optionally be equipped with a power management board. Its function is to take care of the battery pack, providing protection circuits, charger or more precise capacity measurement. A power regulator for the stand-by power line can also be a part of the power manage-

ment board. However, the power management board is not being designed in this thesis as it can be part of future development and it is possible to simply power the onboard avionics system using just a battery pack without other components.

Sometimes it can be beneficial to omit the power management board from the onboard avionics system. In simpler cases such as the Vanguard rocket or rocket for the Czech Rocket Challenge, this allows to minimize mass of the onboard avionics system helping the rocket reach a higher apogee.

2.3.3 Safety and Arming

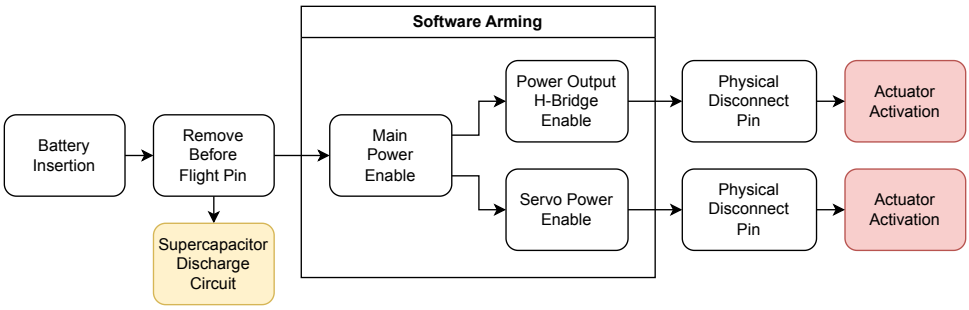

Figure 2.8: Arming System Structure

Safety of the whole system was considered during the design. Arming minimizes the chance of an unsafe or dangerous events occurring due to an anomaly or user error when people are near the rocket. The most dangerous parts of the rocket are typically pyrotechnic actuators or valves operating with high pressure gases. To ensure safe operation, multiple safety features were added to the system and thus failure of a single protection device cannot result in unsafe event occurring.

The arming system structure is described in figure 2.8. The remove before flight (RBF) pin and physical disconnect pins are the most essential parts of the arming procedure. The RBF pin disconnects the main power from the onboard avionics and thus the actuators have no power to operate during the disarmed state. In addition, it activates the supercapacitor discharge circuit to ensure there is no residual charge left. The physical disconnect pins act as a second level of protection. They disconnect the actuators from the power outputs of the onboard avionics. A third level of protection is software arming. There are multiple power switches included in the avionics parts that need to be enabled before power can be passed to the outputs. To further improve safety when working hands on with the avionics system, each power output is equipped with indication light that indicates when the output is powered.

When working on the rocket, all RBF pins and physical disconnect pins shall be inserted. After the rocket is transported to the launch pad and loaded on the launch rail the physical disconnect pins are removed and the launch rail with the rocket is lifted to the upward position. Then the battery

is inserted and a check of all avionics systems is performed. When the rocket is ready for launch the RBF pin shall be removed and all personnel shall leave the launch pad immediately. In case of a rocket with a hybrid fuel engine, the RBF pin is removed prior to the beginning of the tanking process and all personnel leave the launch pad immediately as well. As a last step the software arming is performed and then the rocket is ready for flight. When a person is required to approach the rocket in armed state the RBF pin shall be inserted immediately after approach. Then further disarm actions can be performed depending on the condition of the rocket.

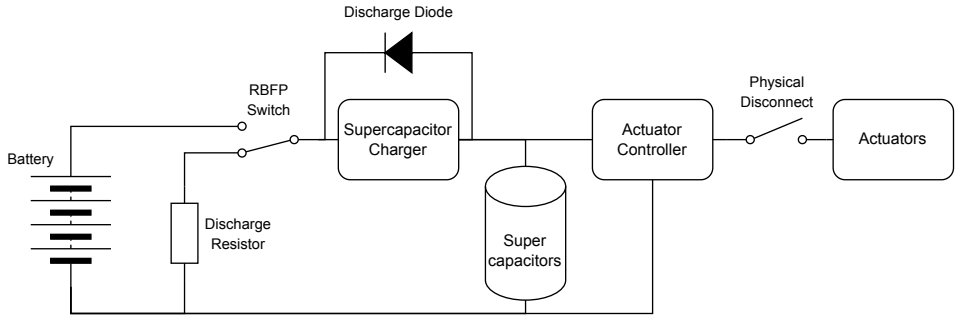

Figure 2.9: Arming Circuit

A simplified arming circuit is shown in figure 2.9. The RBF pin actuates a single-pole double-throw (SPDT) switch that disconnects the main power from the onboard avionics when in disarmed state. It also connects a high power discharge resistor to the power line to discharge all supercapacitors in the onboard avionics system. Each section management board is equipped with a discharge ideal diode to ensure supercapacitor discharge independently of the software state. The discharge resistor value was calculated according to the maximum allowable current on the Rocket Bus to maximize the discharge speed.

There are up to four section management boards expected in large rockets, each equipped with a set of supercapacitors with total capacity of $3.75\,F$. This sums up to $4 \cdot 3.75\,F = 15\,F$ of total capacity in the system. Assuming the avionics operates at $11.4\,V$ nominal voltage and the peak current of the Rocket Bus is $14\,A$, the minimum resistance of the discharge resistor is $R = \frac{U}{I} = \frac{11.4\,V}{14\,A} \doteq 0.814\,\Omega$. A high-wattage resistor with resistance of $R = 1\Omega$ was selected as it is a standard and easily available value. The discharge circuit acts as a first order RC circuit. Therefore the discharge time was calculated as a triple the time constant τ when the voltage of the capacitors reaches $5\,\%$ of the nominal voltage.

$$3\tau = 3 \cdot RC = 3 \cdot 1 \cdot 15 = 45\,s \tag{2.1}$$

In the worst case the rocket is fully disarmed 45 seconds after the RBF pin is inserted. In addition, the flight computer detects the insertion of the RBF pin based on main power line voltage drop and performs a software disarm.

Chapter 3

Flight Computer Design

In this chapter the design process of the flight computer is described. The flight computer was designed to be able to function as a single unit in smaller rockets or as a part of modular avionics system in larger rockets as described in the section 2.3. The design uses commonly available commercial off-the-shelf (COTS) components with components' product lifecycle taken into account to ensure the used components will not be discontinued in the near future. An emphasis was placed on durability of the whole system, therefore the flight computer uses automotive grade components where possible. Automotive grade components can withstand harsh conditions or extended temperature range and are thoroughly tested by the manufacturer to comply with specifications [14]. ESD protection was taken into account as well and all user accessible connectors are equipped with transient voltage suppressors (TVS).

3.1 Flight Computer Architecture

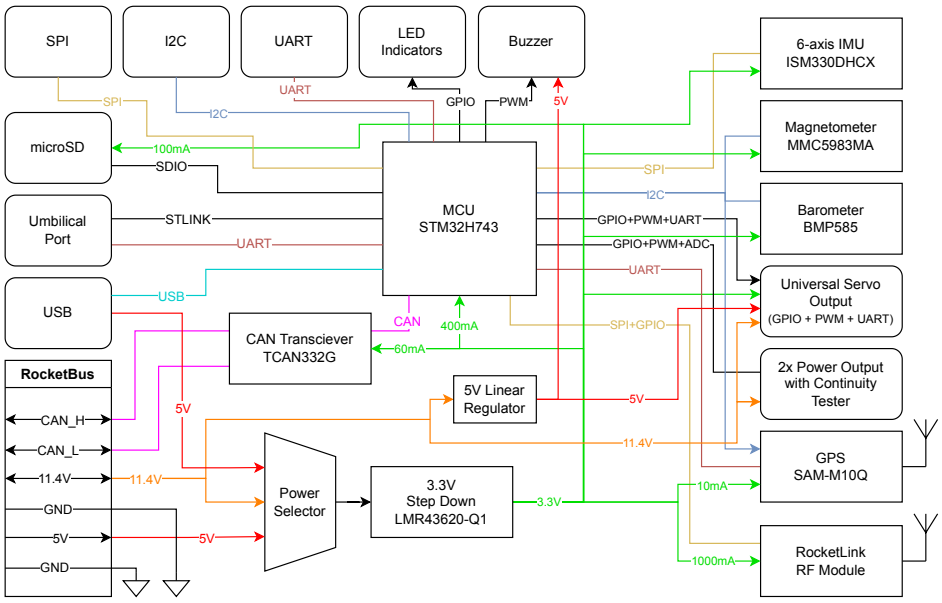

Figure 3.1: Flight Computer Block Diagram

The flight computer block diagram is shown in figure 3.1. The microcontroller (MCU) acts as the main processing unit which is responsible for running the flight software, reading sensor inputs and controlling actuator outputs. It communicates with sensors and power outputs through serial buses such as SPI, I2C or UART and general purpose input-output (GPIO) pins with PWM signal capability. The majority of components is supplied with $3.3\,V$ voltage regulated by a step-down switching power supply. The power supply includes a power selector that autonomously chooses power input from available power sources. Additionally, some serial buses are brought out to connectors to allow for expansion in the future.

3.2 Microcontroller

The selection of the main microcontroller was limited by requirements described in section 2.1.4. The first requirement is the use of microcontroller from STM32 family. Another requirement is the ability to run PX4 RTOS and to run Matlab generated software. This limits the number of options. The PX4 RTOS supports STM32F4, STM32F7 and STM32H7 series of microcontrollers [15]. The Matlab Embedded Coder supports wider variety of microcontrollers, however, the Simulink Coder supports only a limited set [16].

Computing speed and inclusion of a floating-point unit was considered during the selection process, because state estimation and control algorithms will be running on the microcontroller. PX4 RTOS benefits from larger memory, both program and random-access, because operating system presents additional overhead.

From the available options the STM32H743 microcontroller family was selected. It is fully supported by PX4 as well as the underlying NuttX RTOS [17]. Both Matlab Embedded Coder and Simulink Coder can generate software for this microcontroller. It features ARM Cortex-M7 core clocked up to $480\,Mhz$ with floating-point unit and DSP instructions. Large program memory ($2\,MB$) and random-access memory ($1\,MB$) are included as well [18]. STM32H743VI was used as it is the smallest variant with enough pins for all components on the board. It uses LQFP100 package that is easily solderable by hand. The used pin assignment is shown in the figure 3.2.

Assignment of the pins was done taking physical layout of components on the board into account. Firstly, the preliminary board layout with critical components was created. Based on that, pins and peripherals for most critical parts were assigned to simplify the signal path routes on the board. Then signals for all other components were assigned respecting their position relative to the microcontroller.

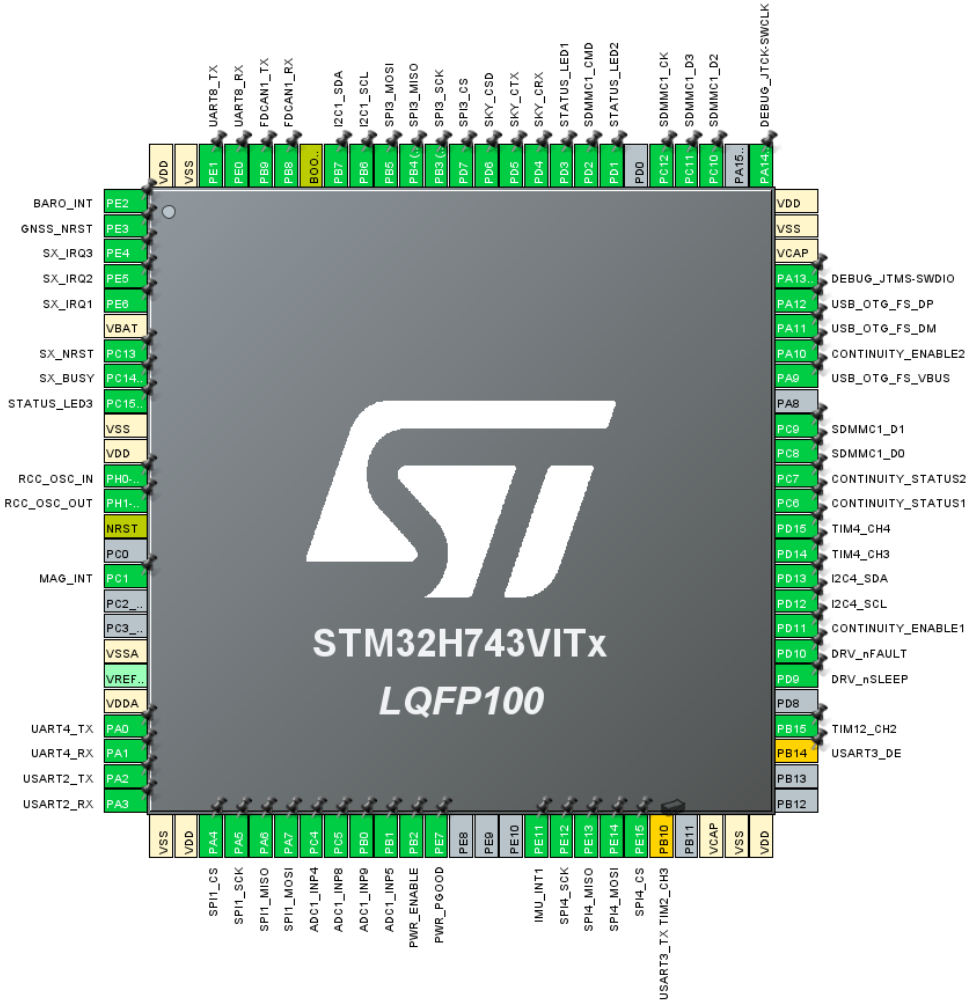

Figure 3.2: Flight Computer Microcontroller Pins Assignment

Decoupling capacitors were added according to manufacturer recommendations [18] as shown in figure 3.3. The analog power supply is connected through ferrite bead $L1$ to filter out high frequency noise from digital circuits improving analog-to-digital converter (ADC) performance. In addition, a solder jumper $JP1$ was added to allow selection of ADC voltage reference between power supply voltage and microcontroller's internal voltage reference source. The MCU internal voltage reference is independent of the main power supply and as a result the ADC can perform better in case of main power supply voltage fluctuations.

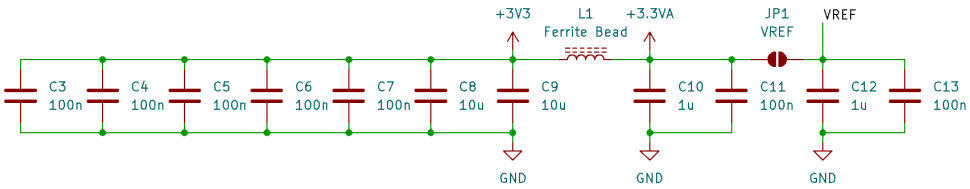

Figure 3.3: Power Supply Scheme for Flight Computer MCU

3.2.1 Clock Source

External crystal is used as clock source for the microcontroller. The oscillator circuit in the microcontroller requires critical crystal transconductance to be less than $G_m = 1.5\,mA/V$. The crystal was selected to fulfill this requirement. Its parameters are described in table 3.1. The stray capacitance C_{stray} was estimated to be $5\,pF$.

Parameter	Value
Fundamental Frequency f	$8\,MHz$
Load Capacitance C_{load}	$8\,pF$
Shunt Capacitance C_{shunt}	$5\,pF$
Equivalent Series Resistance R_{ESR}	$100\,\Omega$
Maximum Drive Level DL_{max}	$300\,\mu W$
Frequency Tolerance	$30\,ppm$
Frequency Stability	$50\,ppm$

Table 3.1: Used Crystal Parameters

Firstly, the minimal critical transconductance for stable oscillation was calculated using formula 3.1 according to manufacturer recommendations[19].

$$g_{mcrit} = 4 \cdot R_{ESR} \cdot (2\pi \cdot f)^2 \cdot (C_{shunt} + C_{load})^2 \tag{3.1}$$

$$g_{mcrit} = 4 \cdot 100 \cdot (2\pi \cdot 8 \cdot 10^6)^2 \cdot \left(5 \cdot 10^{-12} + 8 \cdot 10^{-12}\right)^2 \doteq 0.171\,mA/V \tag{3.2}$$

The calculated minimal critical gain $g_{mcrit} = 0.171\,mA/V$ is lower than maximum crystal transconductance $G_m = 1.5\,mA/V$ and therefore the crystal fits the requirements.

Then worst case drive level DL of the crystal was estimated to avoid overdriving the crystal following equation 3.3 [19].

$$DL = \frac{R_{ESR} \cdot (\pi f \cdot (C_{load} + C_{stray}/2))^2 \cdot V_{pp}^2}{2} \tag{3.3}$$

$$DL = \frac{100 \cdot \left(\pi \cdot 8 \cdot 10^6 \cdot \left(8 \cdot 10^{-12} + \frac{5 \cdot 10^{-12}}{2}\right)\right)^2 \cdot 3.3^2}{2} \doteq 37.9\,\mu W \tag{3.4}$$

The calculated worst case drive level $DL = 37.9\,\mu W$ does not exceed maximum drive level $DL_{max} = 300\,\mu W$, thus the crystal can be used.

As the last step of the crystal circuit design process, external capacitor value C_L for correct crystal load capacitance was calculated according to equation 3.5 [19].

$$C_{L1} = C_{L2} = 2 \cdot (C_{load} - C_{stray}) = 2 \cdot \left(8 \cdot 10^{-12} - 5 \cdot 10^{-12}\right) = 6\,pF \tag{3.5}$$

Crystal frequency tolerance and stability over operating temperature range was considered during component selection as well. CAN bus will be used

as main communication bus between components inside the rocket and it requires certain frequency tolerance to work reliably. According to article [20] CAN bus requires oscillator circuit tolerance as low as 0.3 % when operating at high transmission rates. The selected crystal fulfills this requirement with large safety margin to account for passive components tolerances and parasitic effects of the board layout.

3.3 Sensors

Sensors are a crucial part of the flight computer, because the flight computer performs actions based on input from those sensors. Therefore the sensors were carefully selected from available options on the market. One of the limiting factors was price of the components as the flight computer will be produced by the student team with limited budget. In addition, the rocket is designed and manufactured by students and it may not be one hundred percent reliable. A failure could occur resulting in loss of the vehicle and use of more expensive sensors may negatively affect the team's budget. As a result, sensors with higher price usually aimed at aviation or defense applications were excluded.

Sensors designed for consumer, industrial and drone applications were considered. From available components on the market, few candidates were selected that fit requirements presented in section 2.1. Then a sensor selection process using weighted sum model (WSM) was carried out. Qualitative properties were graded on scale of 1 to 5 (1 - worst, 5 - best), while quantitative properties were compared to each other directly. Based on result of the weighted sum model, the most suitable sensor was used. In addition, sensors previously used in team's avionics systems were included in the weighted sum model to compare their performance against new sensors.

I2C and SPI interfaces are used for communication with the sensors. Pull-up resistors are included for I2C interface. Resistance of 2.2 $k\Omega$ was selected as it enables the bus to operate in Fast mode [21].

3.3.1 Barometer

Barometer is one of the most important sensors in the flight computer. It is used for apogee detection and altitude estimation which is essential for correct recovery system deployment. As described in section 2.1, the barometer must be able to measure altitudes up to 9 km. Altitude h can be estimated from ambient air pressure $p\,[Pa]$ by equation 3.6 published by the National Oceanic and Atmospheric Administration [22] and adjusted for metric units.

$$h = 44307.694 \cdot \left[1 - \left(\frac{p}{101325}\right)^{0.190284}\right] [m] \tag{3.6}$$

From this equation, the required sensor pressure range can be determined.

$$p = 101325 \cdot \left(1 - \frac{h}{44307.694}\right)^{\frac{1}{0.190284}} [Pa] \tag{3.7}$$

$$p = 101325 \cdot \left(1 - \frac{9000}{44307.694}\right)^{\frac{1}{0.190284}} \doteq 30.725\,kPa \tag{3.8}$$

Therefore, barometers that can measure pressure as low as $30\,kPa$ were considered only. The weighted sum model used for barometer selection is shown in table 3.2. Sensor noise performance and absolute pressure accuracy were main factors when selecting the sensor. The level of internal processing features was also considered, because of team's past experience. The MS5637 sensor was used in previous flight computer developed by CTU Space Research and because it features minimal internal processing only, it required more complex communication scheme that resulted in poor performance. In addition, sensor power supply voltage was considered as well, because logic components in the flight computer operate at $3.3\,V$ and a sensor with different supply voltages needs additional power supplies and communication voltage level shifters.

	Weight	MS5637			ICP-101xx			ILPS28QSW			BMP581			BMP585			MS5611		
Power supply voltage [V]	15%	1.5-3.6	5	1.00	1.8	2	0.40	1.7-3.6	5	1.00	1.7-3.6	5	1.00	1.7-3.6	5	1.00	1.8-3.6	5	1.00
Resolution [Pa/LSB]	5%	0.012		0.60	0.010		0.71	0.024		0.30	0.016		0.44	0.016		0.44	0.007		1.00
RMS noise at 100sps [Pa]	25%	2.10		0.14	1.60		0.19	1.14		0.26	0.30		1.00	0.30		1.00	1.80		0.17
Abs. pressure accuracy [±Pa]	25%	400		0.19	150		0.50	100		0.75	75		1.00	85		0.88	350		0.21
Abs. temperature accuracy [±°C]	3%	2.0		0.20	0.4		1.00	1.5		0.27	0.5		0.80	0.7		0.57	2.0		0.20
Embedded features	25%	Minimal	1	0.20	Minimal	1	0.20	Medium	3	0.60	Advanced	4	0.80	Adv.+Rugged	5	1.00	Minimal	1	0.20
Operating temperature range [°C]	2%	-40 to +85	3	0.60	-40 to +85	3	0.60	-40 to +105	4	0.80	-40 to +85	3	0.60	-40 to +85	3	0.60	-40 to +85	3	0.60
		Total:		**0.33**			**0.36**			**0.59**			**0.91**			**0.92**			**0.36**

Table 3.2: Barometer WSM Selection

From the WSM selection process, the BMP585 comes up as the most suitable sensor as it features low noise and high accuracy combined with advanced internal processing features and humidity-resistant rugged design.

The sensor circuit is shown in figure 3.4. Decoupling capacitors were added according to manufacturer recommendations [23]. Additional bulk capacitor was added as well. By connecting the CSB pin to $3.3\,V$, the I2C communication interface is selected. The SDO pin is connected to $3.3\,V$ to choose I2C address 0x47. The sensor is connected to I2C bus and the interrupt output is connected directly to the microcontroller. A large pull-down resistor is added to the interrupt output to prevent it from floating during start-up as it might cause excessive power consumption and false interrupt triggering.

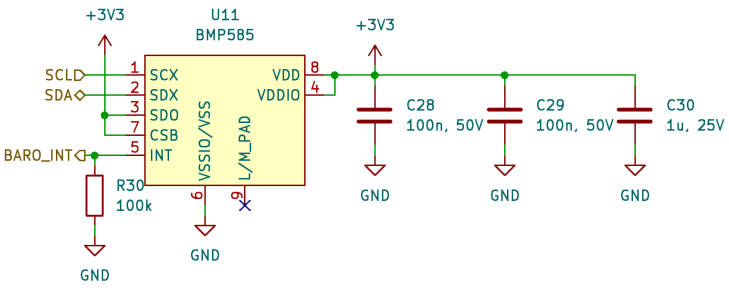

Figure 3.4: Barometer Sensor Circuit

3.3.2 Inertial Measurement Unit

Inertial measurement unit (IMU) is essential for state estimation algorithms as it measures acceleration and angular velocity. 6-axis IMU is preferred compared to separate accelerometer and gyroscope, because the IMU takes up less space on the board. It can offer better axis alignment without complex calibration and better synchronization of measurements. Some models also include sensor data fusion processing unis.

As described in section 2.1, maximum acceleration expected during the flight is $80\,m/s^2$. Therefore, IMUs capable of measuring acceleration of at least $160\,m/s^2 \approx 16\,g$ were considered to gain some margin. High rotational speeds are not desirable in flight and peak rotation measured during previous flights of Illustria rocket was around $800\,°/s$.

The weighted sum model was used for IMU selection as is shown in table 3.3 for accelerometer and table 3.4 for gyroscope separately. Sensor noise performance was main factor when selecting the sensor. Temperature stability of the sensors was also considered, because there can be substantial temperature swings inside the rocket. When standing on the launch pad, the rocket is heated by the sun and interior temperature can reach up to $50\,°C$, but during flight the rocket is cooled by air flow and the sensors cool down quickly. Sensors KX134-1211 and IAM-20380HT were used in previous flight computer developed by CTU Space Research and are present in the WSM for comparison. Few 9-axis IMUs are available on the market such as ICM-20948 or BNO055, however, they offer worse performance than 6-axis IMUs.

	Weight	KX134-1211		ISM330DHCX		BMI088		ICM-40609-D		ICM-20948		BNO055	
Zero-g offset [mg]	5%	75	0.13	10	1.00	20	0.50	40	0.25	50	0.20	80	0.13
Zero-g offset tempco [mg/°C]	15%	0.50	0.20	0.10	1.00	0.20	0.50	0.15	0.67	0.80	0.13	1.00	0.10
Sensitivity [mg/LSB] (16g)	5%	0.49	1.00	0.49	1.00	0.73	0.67	0.49	1.00	0.49	1.00	1.00	0.49
Sensitivity tempco [%/°C]	15%	0.010	0.20	0.005	0.40	0.002	1.00	0.007	0.29	0.026	0.08	0.030	0.07
Range [g]	10%	64	1.00	16	0.25	24	0.38	32	0.50	16	0.25	16	0.25
Power supply voltage [V]	5%	1.7-3.6	5 1.00	1.7-3.6	5 1.00	2.4-3.6	5 1.00	1.7-3.6	5 1.00	1.7-1.95	2 0.40	2.4-3.6	5 1.00
Noise density at 10Hz [µg/√Hz]	30%	300	0.20	60	1.00	190	0.32	100	0.60	230	0.26	150	0.40
Operating temperature range [°C]	5%	-40 to +105	4 0.80	-40 to +105	4 0.80	-40 to +85	3 0.60	-40 to +85	3 0.60	-40 to +85	3 0.60	-40 to +85	3 0.60
Cross axis sensitivity [%]	10%	2.0	0.25	0.5	1.00	0.5	1.00	1.0	0.50	2.0	0.25	1.0	0.50
		Total:	**0.39**		**0.83**		**0.60**		**0.57**		**0.27**		**0.33**

Table 3.3: Accelerometer WSM Selection

	Weight	IAM-20380HT		ISM330DHCX		BMI088		ICM-40609-D		ICM-20948		BNO055	
Zero-rate offset [dps]	5%	0.8	1.00	1.0	0.80	1.0	0.80	1.0	0.80	5.0	0.16	1.0	0.80
Zero-rate offset tempco [dps/°C]	15%	0.007	0.73	0.005	1.00	0.015	0.33	0.010	0.50	0.050	0.10	0.015	0.33
Sensitivity [dps/LSB] (2000dps)	5%	0.061	1.00	0.070	0.87	0.061	1.00	0.061	1.00	0.061	1.00	0.063	0.98
Sensitivity tempco [%/°C]	15%	0.010	0.70	0.007	1.00	0.030	0.23	0.045	0.16	0.024	0.29	0.030	0.23
Range [dps]	10%	2000	0.50	4000	1.00	2000	0.50	2000	0.50	2000	0.50	2000	0.50
Power supply voltage [V]	5%	1.7-3.6	5 1.00	1.7-3.6	5 1.00	2.4-3.6	5 1.00	1.7-3.6	5 1.00	1.7-1.95	2 0.40	2.4-3.6	5 1.00
Noise density at 10Hz [mdps/√Hz]	30%	5.0	0.90	5.0	0.90	14.0	0.32	4.5	1.00	15.0	0.30	14.0	0.32
Operating temperature range [°C]	5%	-40 to +105	4 0.80	-40 to +105	4 0.80	-40 to +85	3 0.60	-40 to +85	3 0.60	-40 to +85	3 0.60	-40 to +85	3 0.60
Cross axis sensitivity [%]	10%	1.0	1.00	1.0	1.00	1.0	1.00	1.0	1.00	2.0	0.50	1.0	1.00
		Total:	**0.82**		**0.94**		**0.50**		**0.72**		**0.36**		**0.50**

Table 3.4: Gyroscope WSM Selection

After comparing accelerometers and gyroscopes separately, their results are combined into a single result characterizing whole IMU as shown in table 3.5. ISM330DHCX comes out of the selection process as the most suitable IMU for this application. It offers good noise performance and temperature stability compared to other options. It is also an improvement over previously used components.

	Weight	KX134-1211 IAM-20380HT	ISM330DHCX	BMI088	ICM-40609-D	ICM-20948	BNO055
Gyroscope	50%	0.39	0.83	0.60	0.57	0.27	0.33
Accelerometer	50%	0.82	0.94	0.50	0.72	0.36	0.50
Total:		**0.61**	**0.88**	**0.55**	**0.64**	**0.31**	**0.42**

Table 3.5: Inertial Measurement Unit WSM Selection Result

Sensor circuit is shown in figure 3.5. Decoupling capacitors were added according to manufacturer recommendations [24]. Dedicated SPI communication interface is used for the IMU to allow high speed data transfer. Pull-up resistor is included on the chip-select line to prevent it from floating during start-up. The CS pin also selects between SPI and I2C modes of the sensor. Interrupt pin is connected to the MCU for more efficient interrupt-based data retrieval. The interrupt pin includes an embedded pull-down resistor in the sensor. Auxillary interface pins SDx, SCx, OCS_Aux and SDO_Aux are not used and therefore are connected to ground or left disconnected based on manufacturer's instructions. Sensor Hub feature that can collect data from other sensors is included in the IMU but it is not used in this application. Direct communication between sensors and MCU is used as it offers higher flexibility.

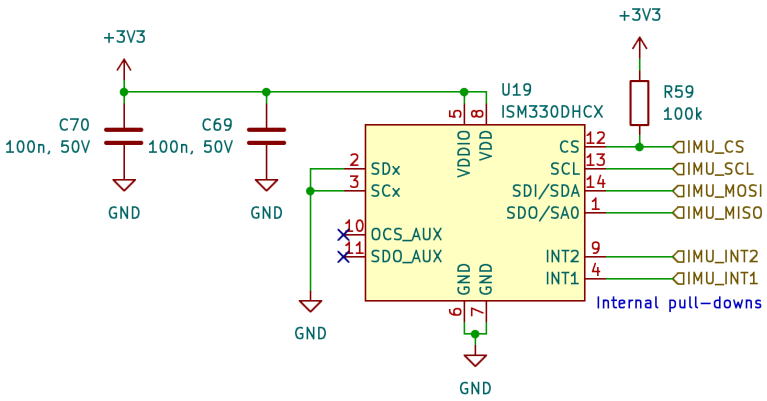

Figure 3.5: Inertial Measurement Unit Sensor Circuit

3.3.3 Magnetometer

Magnetometer is not required by this application, but it can be helpful for state estimation algorithms as it provides compass functionality. Thus it is included in the flight computer.

Selection of the magnetometer was done using weighted sum model as is shown in table 3.6. Measurement noise performance was the main factor

when selecting the sensor. Additionally, sensor linearity was considered as well. Because the sensor will be used as a compass, only small magnetic field measuring range is required and all candidate sensors fulfill this requirement.

	Weight	LIS3MDL		MMC5983MA		BMM350		HMC5883L		BNO055	
Field range [µT]	0%	400		800		2000		800		1300	
Power supply voltage [V]	15%	1.9-3.6	5 1.00	2.8-3.6	5 1.00	1.7-1.9	2 0.40	2.2-3.6	5 1.00	2.4-3.6	5 1.00
RMS Noise at 100sps [nT]	50%	611	0.10	60	1.00	524	0.11	200	0.30	520	0.12
Linearity Error [nT]	20%	1440	0.56	800	1.00	20000	0.04	800	1.00	13000	0.06
Sensitivity [nT/LSB]	10%	14.6	0.42	6.1	1.00	100.0	0.06	73.0	0.08	79.3	0.08
Operating temperature range [°C]	5%	-40 to +85	3 0.60	-40 to +105	4 0.80	-40 to +85	3 0.60	-30 to +85	3 0.60	-40 to +85	3 0.60
		Total:	**0.38**		**0.99**		**0.16**		**0.54**		**0.26**

Table 3.6: Magnetometer WSM Selection

MMC5983MA was selected as it offers the best performance across considered properties compared to all other options. The sensor circuit is shown in figure 3.6. Decoupling capacitors were added according to manufacturer recommendations [25] as well as bulk capacitor. Because the magnetometer uses AMR sensor, it needs large capacity to perform magnetization pulses. The manufacturer recommends using at least $10\,\mu F$ capacitor for this purpose but additional capacity was added to ensure correct operation. The sensor is connected to I2C bus and the interrupt output is connected to the microcontroller for more efficient data retrieval. Pull-down resistor is added to the interrupt line to avoid false triggering during start-up. SPI_CS pin is connected to $3.3\,V$ to select SPI mode. SPI_SDO pin is left disconnected as it is not used in I2C mode.

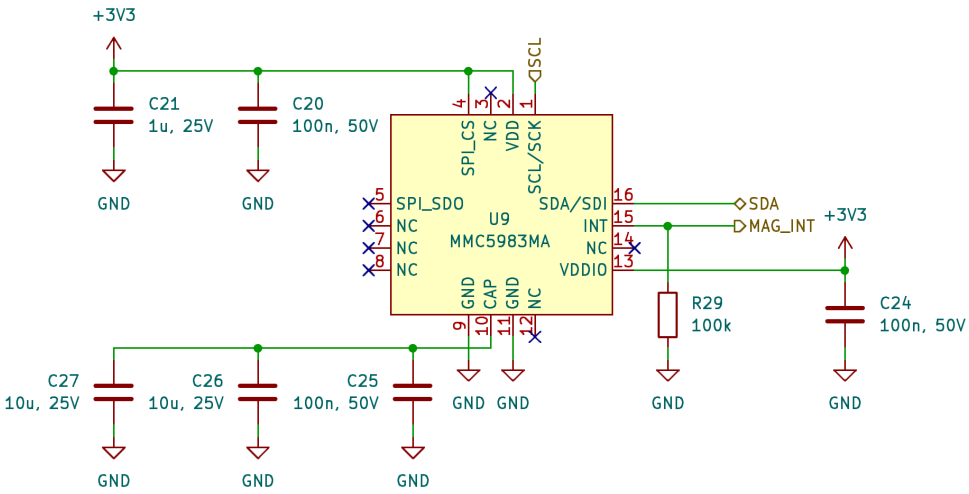

Figure 3.6: Magnetometer Sensor Circuit

3.3.4 GNSS

Global navigation satellite system (GNSS) is used by state estimation algorithms. After landing, it is also used for easier rocket retrieval as it can provide exact coordinates of the rocket.

GNSS radio signals can be very weak and improper layout of traces to the antenna can significantly decrease performance of the GNSS receiver. Wide variety of GNSS receivers are available on the market, however, GNSS receiver module SAM-M10Q was selected as it is a fully integrated solution with an antenna. This avoids the need to design RF traces on the board and thus eliminating the potential issue with signal quality. Per manufacturers recommendations, no parts are placed in the vicinity of the GNSS receiver to minimize interference. A large continuous ground plane surrounds the GNSS receiver for optimal performance [26].

GNSS receiver circuit is shown in figure 3.7. Large bulk capacitor is added to cover current peaks, because the receiver module includes a switching-mode power supply. Both I2C and UART interfaces are connected to the microcontroller, allowing software developers to choose the optimal communication interface. Large pull-up resistors are connected to UART signals to avoid floating state during start-up. Timepulse output is connected to the microcontroller. A timer peripheral in the MCU can be used to count time pulses providing a precise time from GNSS to the flight software. Additionally a reset signal is connected to the microcontroller to allow software to reset the GNSS receiver in case of any issues. The GNSS receiver includes an integrated pull-up resistor for the reset signal.

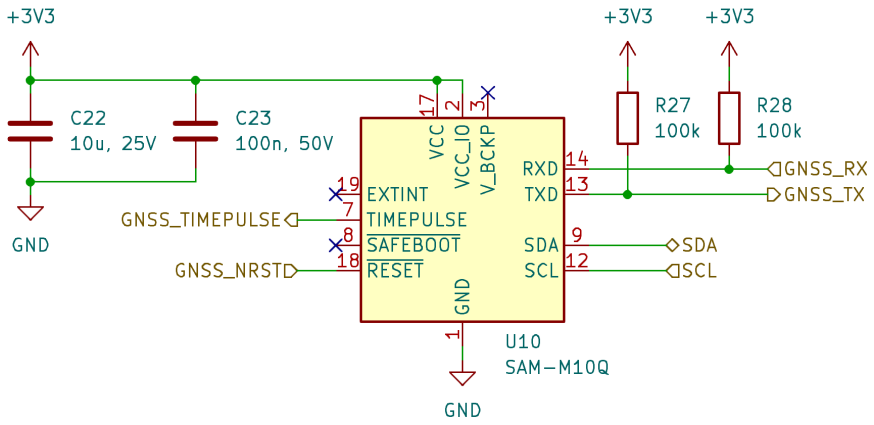

Figure 3.7: Global Navigation Satellite System Receiver Circuit

3.4 Power Management

Power management subsystem in the flight computer delivers power at correct voltages to all components while also protecting from overcurrent events and measuring power input voltage and current. The overview of power management subsystem is shown in figure 3.8. Power is supplied from RocketBus as described in section 2.3.2 through two power lines - high power line and stand-by power line. USB can be also used to power logic components of the flight computer during programming, configuration or data download.

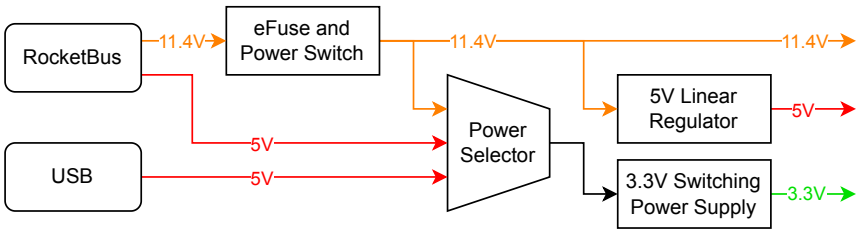

Figure 3.8: Flight Computer Power Management Diagram

High-power line from RocketBus is connected through eFuse and power switch to actuator outputs. It is also used to supply $5V$ linear regulator that provides power for buzzer and servo signal output. All three power inputs are connected to the power selector with included resettable fuses to power $3.3V$ switching power supply. 3.3V power line is then used to power all logic components on the flight computer.

Considering $3.3V$ power line, the RocketLink wireless module has the largest current consumption up to $1\,A$ followed by the microcontroller around $400\,mA$ when clocked at maximum frequency. Other components do not have significant power consumption. Therefore, a switching power supply capable of delivering at least $1.5\,A$ current is required.

3.4.1 Electronic Fuse and Power Switch

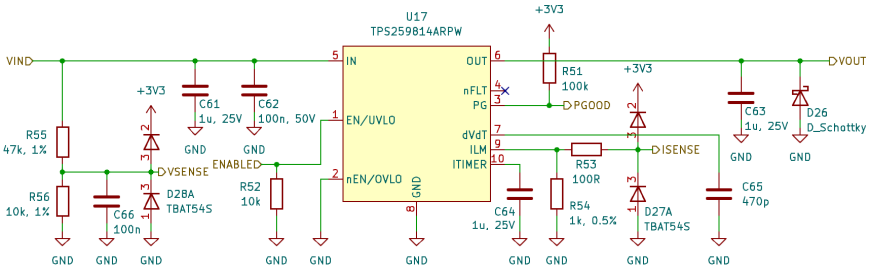

Figure 3.9: Electronic fuse and Power Switch Circuit

Electronic fuse TPS25981 is used for protection of the high-power line against overcurrent events. Simultaneously it also acts as a power switch capable of disconnecting power from actuator outputs. This is useful as an additional layer of safety to avoid unintentional actuator activation. It also helps to reduce power consumption when the rocket is waiting for launch as servo-motors can draw significant amount of power. Electronic fuse is used in this case instead of resettable PTC fuses because PTC fuses tend to have larger footprint with higher trip current ratings and they are heavily dependant on ambient temperature [27]. Electronic fuses also provide additional features compared to PTC fuses.

The circuit is shown in figure 3.9. Current limit is set by resistor $R54$ according to formula 3.9 [28]. Maximum current $I_{lim} = 6\,A$ was chosen. This

is enough for a servomotor as well as for ignition of pyrotechnic charges.

$$R_{ILM} = \frac{6585}{I_{lim}} = \frac{6585}{6} = 1097.5\,\Omega \tag{3.9}$$

Commonly available value of resistor $R54 = 1\,k\Omega$ was selected instead as a close approximation. This changes the real current limit to $I_{lim} = \frac{6585}{1000} = 6.585\,A$. If necessary, the current limit can be increased up to $10\,A$ by changing the $R54$ resistor value accordingly.

The ILM output functions as a current measurement output as well. Voltage U_{ILM} measured at the ILM output is proportional to the current I_{load} flowing through the electronic fuse according to equation 3.10

$$I_{load} = \frac{U_{ILM}}{G_{imon} \cdot R_{ILM}} = \frac{U_{ILM}}{0.0953}\ \ [A] \tag{3.10}$$

where $G_{imon} = 95.3\,\mu A/A$ is gain of current measurement output. This output is connected through a current limiting resistor $R53$ to AD converter in the microcontroller. Protective serial diodes $D27$ are added to limit input voltage of the AD converter.

In addition the electronic fuse can allow double the maximum current to flow for a limited period of time. Period of $t_{ITIM} = 0.8\,s$ was chosen. This period is set by capacitor $C64$ according to formula 3.11 [28]

$$C_{ITIM} = t_{ITIM} \cdot \frac{I_{ITIM}}{dV_{ITIM}} = 0.8 \cdot \frac{2 \cdot 10^{-6}}{1.51} \doteq 1.06\,\mu F \tag{3.11}$$

where $I_{ITIM} = 2\,\mu A$ and $dV_{ITIM} = 1.51\,V$ are constant parameters of the electronic fuse. Commonly available value of capacitor $C64 = 1\,\mu F$ was selected instead as a close approximation. This changes the real double current period to $t_{ITIM} = C_{ITIM} \cdot \frac{dV_{ITIM}}{I_{ITIM}} = 1 \cdot 10^{-6} \cdot \frac{1.51}{2 \cdot 10^{-6}} = 0.755\,s$.

The electronic fuse provides inrush current control functionality. It is used to limit peak current when the power switch is turned on and capacitors in servomotors are charging. Capacitance that might be connected to the power output can change based on the connected actuators, but it was estimated as $C_{out} = 150\,\mu F$. Inrush current limit of $I_{inrush} = 1\,A$ was chosen. From this, the required slew rate was calculated $SR = \frac{I_{inrush}}{C_{out}} = \frac{1\,A}{150\,\mu F} \doteq 6.6667\,V/ms$. The inrush current limit is set by capacitor $C65$ calculated according to formula 3.12 [28].

$$C_{dV\,dt} = \frac{3.3 \cdot 10^{-6}}{SR} = \frac{3.3 \cdot 10^{-6}}{6666.7} \doteq 494\,pF \tag{3.12}$$

Commonly available value of capacitor $C65 = 470\,pF$ was selected instead as a close approximation.

Overvoltage and undervoltage protections are not used in this application. The undervoltage input is used to control the electronic fuse as a power switch with added pull-down resistor $R52$ to ensure that the power switch is turned off during start-up. PGOOD open-drain output that signalizes state of the electronic fuse is connected to the microcontroller. The electronic fuse

features an internal pull-down resistor that ensures the PGOOD output is pulled low when the fuse is not powered. For that reason only a weak pull-up resistor $R51$ is added to avoid false activation of the output. Capacitors on input and output of the fuse along with a Schottky diode for protection are added according to manufacturer recommendations [28].

Measurement of input voltage is useful for state monitoring and for detection of arming pin insertion as described in section 2.3.3. For this purpose a voltage divider made out of resistors $R55$ and $R56$ is added along with anti-aliasing low-pass RC filter and protection diodes to limit ADC input voltage. Although voltage around $11.4\,V$ is expected on the input high-power line, higher voltage was considered for safety margin. Commonly available resistor values $R55 = 47\,k\Omega$ and $R56 = 10\,k\Omega$ were used for the voltage divider. The resulting voltage division factor is $U_{out} = U_{in} \cdot \frac{R56}{R55+R56} = U_{in} \cdot \frac{10}{57}$ and with maximum ADC input voltage of $3.3\,V$ the maximum measurement range is $3.3 \cdot \frac{57}{10} = 18.81\,V$. Anti-aliasing filter with a precise cutoff frequency is not important in this case and the filter was constructed using a commonly available capacitor value $C66 = 100\,nF$. The cutoff frequency f_{cutoff} is calculated using formula 3.13. Output of the low-pass filter is connected to AD converter in the microcontroller.

$$f_{cutoff} = \frac{1}{2\pi \cdot R55 \| R56 \cdot C66} = \frac{1}{2\pi \cdot \frac{47 \cdot 10^3 \cdot 10^4}{47 \cdot 10^3 + 10^4} \cdot 10^{-7}} \doteq 193\,Hz \qquad (3.13)$$

3.4.2 Power Selector

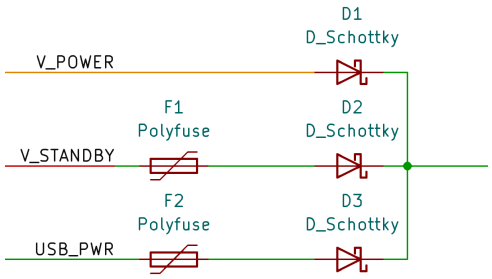

Figure 3.10: Power Selector Circuit

Power selector is used to provide redundant power to logic components and to allow power input from multiple sources simultaneously without backflow to lower voltage supplies. The circuit is shown in figure 3.10. Power selector is formed by parallel connection of Schottky diodes with additional resettable PTC fuses on inputs without overcurrent protection. Selected resettable PTC fuses are sized with a safety margin because their trip current decreases significantly with higher ambient temperature [27].

Power dissipation on the diodes was considered during design. Diodes with forward voltage $U_f = 0.41\,V$ and thermal resistance $R_{ja} = 130\,K/W$ were selected. The power selector supplies power to $3.3\,V$ switching power supply

with estimated efficiency of $\eta = 85\%$. Current output of the $3.3V$ power supply is expected to be $I_{3.3V_{max}} = 1.5\,A$ in the worst conditions when all components on the board are operating at maximum power. However, lower average current around $I_{3.3V_{avg}} = 0.5\,A$ is expected during normal operation. Since a switching power supply is used, the largest current flows when only the lowest voltage power input $U_{in} = 5\,V$ is used. From that, the current flowing through the power selector can be calculated as shown in formulas 3.14 and 3.15.

$$I_{max} = \frac{U_{out}}{\eta \cdot U_{in}} \cdot I_{3.3V_{max}} = \frac{3.3}{0.85 \cdot 5} \cdot 1.5 \doteq 1.16\,A \tag{3.14}$$

$$I_{avg} = \frac{U_{out}}{\eta \cdot U_{in}} \cdot I_{3.3V_{avg}} = \frac{3.3}{0.85 \cdot 5} \cdot 0.5 \doteq 0.39\,A \tag{3.15}$$

Having obtained current values for both maximum and average power inputs, the junction temperatures of the diodes t_{max} and t_{avg} can be calculated using formulas 3.16 and 3.17. Calculations take ambient temperature $t_0 = 50\,°C$ into account.

$$t_{max} = t_0 + U_f \cdot I_{max} \cdot R_{ja} = 50 + 0.41 \cdot 1.16 \cdot 130 \doteq 111.8\,°C \tag{3.16}$$

$$t_{avg} = t_0 + U_f \cdot I_{avg} \cdot R_{ja} = 50 + 0.41 \cdot 0.39 \cdot 130 \doteq 70.8\,°C \tag{3.17}$$

The maximum diode junction temperature $t_{max} = 111.8\,°C$ is relatively high but still falls within operating range of the diode [29]. Furthermore, the circuit is not expected to operate at high current for long periods of time. The average junction temperature $t_{avg} = 70.8\,°C$ is acceptable. To allow better heat dissipation from the power selector, thermal vias are placed near the diodes and are connected to a large copper plane.

3.4.3 3.3V Switching Power Supply

Majority of components on the board are powered by 3.3V switching power supply. For this purpose, LMR43620 synchronous step-down converter is used. It is a highly integrated solution with embedded switching transistors enabling design of high-efficiency power supply with small board footprint. It utilizes spread spectrum switching to reduce electromagnetic interference. This is helpful for good performance of GNSS receiver and telemetry transceiver. High efficiency and small board footprint allows to design smaller board without overheating issues.

Multiple variants of the converter are available and $3.3V$ variant with fixed frequency was selected. It operates at high switching frequency $f_{SW} = 2.2\,MHz$ allowing use of smaller inductor and output capacitors. It is capable of outputting current up to $2\,A$, fulfilling the requirements described in section 3.4. The design is based on recommended design procedure by the manufacturer [30]. Used switching power supply circuit is shown in figure 3.11.

Converter variant with $3.3V$ fixed output voltage was selected, nevertheless, the output voltage can be adjusted. In normal operation, the output voltage

feedback is connected through $0\,\Omega$ resistor $R34$ to the converter feedback input, but footprint for additional resistor $R35$ forming a voltage divider is present in the circuit to allow for adjusting of the output voltage if necessary.

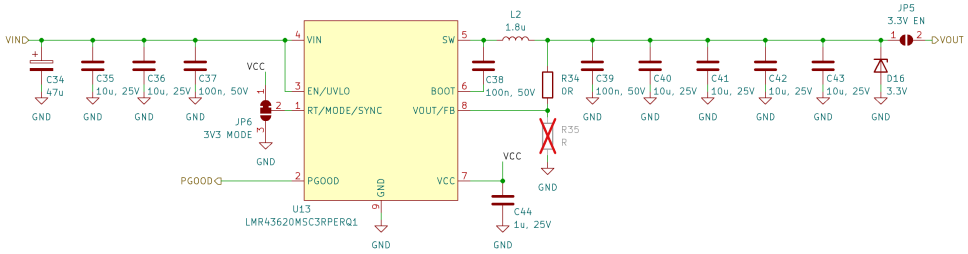

Figure 3.11: 3.3V Switching Power Supply Circuit for Flight Computer

Inductor selection was done in steps. Firstly, the approximate inductor value was estimated based on recommended ripple current percentage $K = 0.3$ by formula 3.18 [30]

$$L = \frac{U_{in} - U_{out}}{f_{SW} \cdot K \cdot I_{max}} \cdot \frac{U_{out}}{U_{in}} \tag{3.18}$$

where U_{in} is the input voltage, $U_{out} = 3.3\,V$ is the output voltage and $I_{max} = 2\,A$ is the maximum output current. Since the input voltage can be in range of $4.5\,V$ to $12\,V$, inductor estimation was done for both extremes to check operating parameters in all conditions.

$$L_{12V} = \frac{12 - 3.3}{2.2 \cdot 10^6 \cdot 0.3 \cdot 2} \cdot \frac{3.3}{12} \doteq 1.81\,\mu H \tag{3.19}$$

$$L_{4.5V} = \frac{4.5 - 3.3}{2.2 \cdot 10^6 \cdot 0.3 \cdot 2} \cdot \frac{3.3}{4.5} \doteq 0.67\,\mu H \tag{3.20}$$

Then the maximum duty cycle D for both extremes was calculated with formula 3.21 [31].

$$D = \frac{U_{out}}{U_{in} \cdot \eta} \tag{3.21}$$

$$D_{12V} = \frac{3.3}{12 \cdot 0.85} \doteq 0.324 \tag{3.22}$$

$$D_{4.5V} = \frac{3.3}{4.5 \cdot 0.85} \doteq 0.863 \tag{3.23}$$

Based on the duty cycle and inductor values, real current ripple was estimated with formula 3.24 [31].

$$I_{ripple} = \frac{(U_{in} - U_{out}) \cdot D}{f_{SW} \cdot L} \tag{3.24}$$

Calculated results are in table 3.7. The converter requires minimal current ripple to be at least 10% of the maximum output current or at least $0.2\,A$ in this case. Maximum current ripple is limited by switching transistor peak current limit, which is $2.8\,A$ in this case. This limit is a sum of output current and current ripple. Due to those limitations, inductor with $L = 1.8\,\mu H$

U_{in} $[V]$	L $[\mu H]$	D $[-]$	I_{ripple} $[A]$
4.5	1.81	0.863	0.26
4.5	0.67	0.863	0.70
12	1.81	0.324	0.71
12	0.67	0.324	1.91

Table 3.7: Calculated current ripple for 3.3V FC power supply

inductance was selected as it is a commonly available value and it fits within the presented limitations. Inductor with metal alloy powder and with high saturation current of $3.4\,A$ is used to avoid risk of core saturation and potential failure of the power supply.

Output capacity around $44\,\mu F$ with small ESR is recommended by the manufacturer. This was achieved by using four ceramic capacitors with $10\,\mu F$ capacity. Additional $100\,nF$ capacitor is used to reduce voltage spikes caused by inductor and board parasitics [30]. Capacitors with high voltage rating of $25\,V$ were used in the design because multilayer ceramic capacitors with X7R dielectric lose significant percentage of capacity with higher charge voltage [32].

Input capacitors were added according to manufacturer recommendations [30]. Two ceramic capacitors with $10\,\mu F$ capacity were used along with a $100\,nF$ capacitor as a high frequency bypass for converters's internal control circuits. Additional $47\,\mu F$ tantalum capacitor is used as its higher ESR can help dampen ringing on input supply with long power leads.

Jumper JP6 is used to select control mode of the power supply. It can operate in fixed PWM (FPWM) mode or in automatic mode that chooses between FPWM and pulse frequency modulation (PFM) modes based on load. FPWM mode is selected by default in the design because PFM mode can generate electromagnetic interference on unpredictable frequencies and can negatively affect wireless receivers performance. However, this comes with a cost of lower efficiency in lower loads.

$3.3V$ Zener diode is added to the output of the power supply to protect against over-voltage that might be caused by current backflow through protection diodes. Jumper $JP5$ is used mostly during board testing. It allows to disconnect sensitive components from the power supply and to measure output current. Since the power supply is the main supply for the microcontroller, PGOOD output is used as a reset signal. This ensures that the power supply is fully started and stable before enabling the microcontroller.

Relation between power supply current I_{out} and junction temperature t_j is described by equation 3.25 [30]

$$I_{out} = \frac{t_j - t_a}{R_{ja}} \cdot \frac{\eta}{1-\eta} \cdot \frac{1}{U_{out}} \tag{3.25}$$

where $t_a = 50\,°C$ is ambient air temperature, $U_{out} = 3.3\,V$ is output voltage, $\eta = 85\%$ is power supply efficiency and $R_{ja} = 84.4\,K/W$ is thermal resistance of the package.

From that equation, the converter junction temperature can be estimated.

$$t_j = I_{out} \cdot R_{ja} \cdot \frac{1-\eta}{\eta} \cdot U_{out} + t_a = 2 \cdot 84.4 \cdot \frac{1-0.85}{0.85} \cdot 3.3 + 50 = 148.3\,°C \quad (3.26)$$

The resulting junction temperature $t_j = 148.3\,°C$ is right at the edge of operating conditions of the converter. However, these calculations estimate the worst case scenario and the converter is expected to operate at lower currents. Thermal vias connected to a large copper plane are placed under and around the converter for better heat dissipation.

3.4.4 5V Linear Power Supply

Servo signal logic output and buzzer requires 5V power supply. This is provided by linear low-dropout (LDO) regulator AP7370-50FDC. It features integrated short current, reverse current and thermal protections. The regulator is powered from the high power line. Input and output capacitors are added according to manufacturer recommendations [33] as shown in figure 3.12. On the input there is solder jumper $JP8$ that can be used to turn off the power supply. On the output there is a $5.1\,V$ Zener diode connected that protects the power rail from over-voltage that might be caused by current backflow through output protection diodes.

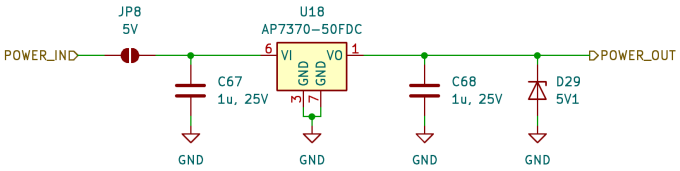

Figure 3.12: 5V Linear Power Supply Circuit

The linear regulator has thermal resistance of $R_{ja} = 54\,K/W$. With maximum input voltage of $U_{in} = 11.4\,V$, output voltage of $U_{out} = 5\,V$ and peak output current $I_{out} = 0.15\,A$, the junction temperature t can be calculated using the formula 3.27. Ambient temperature $t_0 = 50\,°C$ is taken into account.

$$t = t_0 + (U_{in} - U_{out}) \cdot I_{out} \cdot R_{ja} = 50 + (11.4 - 5) \cdot 0.15 \cdot 54 \doteq 101.8\,°C \quad (3.27)$$

The junction temperature $t = 101.8\,°C$ falls within operating range of the linear regulator. Thermal vias connected to a large copper plane are placed under the linear regulator to help with heat dissipation.

3.5 Actuator Outputs

The flight computer is equipped with multiple actuator outputs. Servomotor, solenoid, glow wires or pyrotechnic charges can be operated by the flight computer. Due to that, the flight computer can control simpler rockets all by itself.

3.5.1 Servo Output

Servo output is designed to be flexible to accommodate various types of servo control protocols. As described in section 2.1, the flight computer needs to be able to control both PWM controlled and digital serial bus controlled servomotors. Serial bus servomotors are becoming more common and are available from multiple manufacturers. However, they lack standardization as each manufacturer defines their own protocol and physical interface. A common element among many manufacturers is use of some variant of single-wire UART communication. Those servomotors usually use 3 wire connectors similarly to PWM controlled servomotors. Servomotors using RS485 bus are also available on the market but those were left out of the design, because they are not backwards compatible with PWM signal output and CTU Space Research intends to use servomotors controlled with single-wire UART in the future.

Because multiple manufacturers such as Waveshare [34], Hiwonder [35] and Futaba [36] use single-wire UART communication with slightly different physical interface, circuit in figure 3.13 was designed to accommodate for those differences. The manufacturer recommended bus driver circuit usually consists of a pair of logical buffer gates with different operating voltages and different pull-up or pull-down resistor configuration. Since the communication is half-duplex, the driver circuits include a direction selection input driven by the microcontroller that enables or disables the transmitter based on the required data direction.

For this purpose the SN74LXC1T45-Q1 bidirectional bus driver with voltage level shifting capability was used. The driver can output up to $30\,mA$ current. It integrates both required logic buffer gates into a single package and solves the issue with different logic voltages used by different manufacturers. Solder jumper $JP7$ is used to select correct logic voltage between $3.3\,V$ and $5\,V$.

Various supporting components were added to the output to accommodate for different physical servo interfaces, to increase robustness of the output and to add other function modes. The signal and power traces are protected from ESD discharge by TVS diodes. Pull-up or pull-down resistors $R47$ and $R50$ can be installed by the user according to requirements of the used servomotor. Over-voltage protection in form of two serial Schottky diodes with current limiting resistor $R49$ is also added. Capacitor $C60$ can be installed to form a low-pass filter on input or output. That can be used to eliminate bouncing of switches when the circuit is used as digital input.

Pin assigned in the microcontroller for servo output was chosen carefully to support different function modes. Pin that supports single-wire UART communication, PWM signal generation and digital input and output is used. Because the single-wire UART peripheral in the microcontroller is designed as open-drain output, additional pull-up resistor $R46$ is added. The UART peripheral is able to generate direction signal and it was used as direction input for the bus driver circuit simplifying the software operations.

As a result a complex bus driver circuit is designed that can operate in multiple modes. It can act as a simple digital input or output that can

be used for switch state sensing. It can generate PWM signal for classical servomotor control or count incoming pulses and their lengths using timer peripheral. It can also act as a single-wire UART communication interface for serial servomotor control. The servo output uses Molex KKPLUS250 connector as described in section 2.3.1.

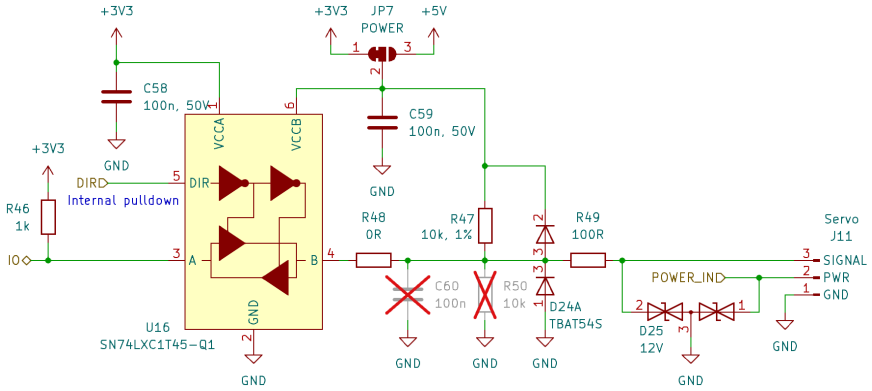

Figure 3.13: Servo Output Circuit

3.5.2 High-power Outputs

High-power outputs are used for pyrotechnic charge ignition or for glow-wires. A solenoid can be connected to the output as well. The circuit in figure 3.14 is used for this purpose. It features an integrated H-bridge circuit DRV8256 capable of outputting up to $6\,A$ of current. It can operate at various voltages starting at $4.5\,V$. Decoupling capacitors are added according to manufacturer's recommendations [37]. Advanced features of the H-bridge such as decay mode or smart tune are not used in this application and are left at default settings.

The H-bridge includes thermal, undervoltage and overcurrent protections. Output current limitation can be set to a lower value if needed by adjusting resistors $R36$ and $R37$. High-power outputs are controlled with two digital inputs connected to timer peripheral in the microcontroller as it can generate pulses with defined length independent on the software. Sleep signal input and fault output are connected to the microcontroller. The driver needs to be enabled by the sleep input first before any output can be activated. This serves as another layer of safety to avoid accidental activation of connected actuators. Additional capacitor and resistor is added to the sleep input forming RC circuit. This minimizes the risk of false activation caused by electromagnetic interference. Fault signal indicates any issues with the H-bridge such as overcurrent or thermal shutdown to the microcontroller. It is an open-drain output and thus a pull-up resistor is added.

The H-bridge can operate as two separate half-bridges. This feature is used to drive two independent outputs with a single chip, because glow-wires or pyrotechnic charges are independent on polarity of the output. However, full H-bridge can be utilized as well to drive a solenoid where the polarity can be important. In half-bridge mode, the load is connected between driver

output and ground and the driver operates as a high-side switch. This minimizes the risk accidental activation of actuators during manipulation with cables, because high-power line is not connected to the load in inactive state in contrast to low-side switches. In case of half-bridge mode, the load is connected between terminals 1 and 2 or 3 and 4. In case of full-bridge mode, the load is connected between terminals 2 and 3. LEDs are connected to the outputs to signalize whether power is being applied to the outputs or not.

Screwless terminal block with push button clamp is used for connection of actuators to high-power outputs. This solution was selected to improve user-friendliness when used with smaller rockets, because pyrotechnic charges are consumable equipment and they need to be replaced after use. Terminal block simplifies this process as there is no need to reattach a connector each time. Power outputs on the flight computer are not intended to be used for larger rockets where section management boards are present.

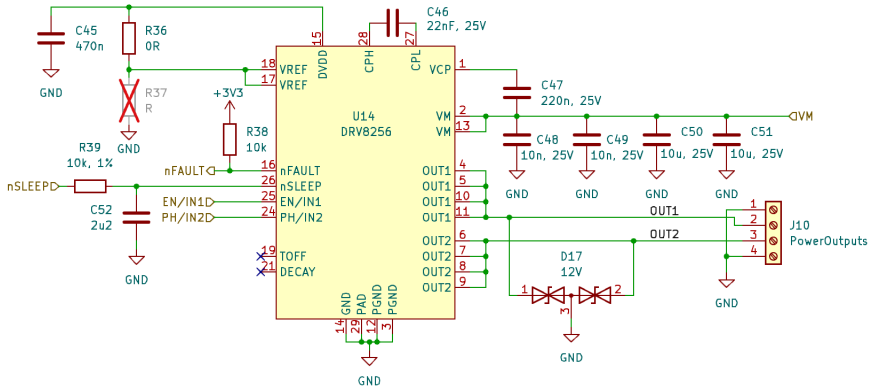

Figure 3.14: High-power Outputs Circuit

Continuity Tester

Simple continuity test circuit is added to the power outputs as shown in figure 3.15. It can be used to check if the load is connected correctly by testing continuity between output and ground through the load. The test circuit can be used only in half-bridge output mode.

It checks continuity by passing small current through the load and measuring if current is flowing or not. The current is sourced from microcontroller pin. This is useful because the continuity test can be enabled and disabled easily. Current flows through a sense resistor, diode and the load to ground. Voltage drop on the sense resistor is measured with AD converter in the microcontroller and based on the measurement the continuity status is determined. Resistors $R40$ and $R41$ and diodes $D20$ and $D21$ are used for this purpose depending on which output is being tested. Diodes $D20$ and $D21$ serve as protection of microcontroller to block high voltage present on power outputs when activated. Serial diodes $D18$ and $D19$ act as a second layer of protection to limit input voltage range to safe levels for microcontroller and to dissipate any leakage current from diodes $D20$ and $D21$. In addition, indicator LEDs

operated by the microcontroller are used to indicate if loads are connected correctly.

Maximum current flowing through the load when load resistance $R_{load} = 0\,\Omega$ can be calculated using formula 3.28

$$I_{max} = \frac{U_{enable} - U_D}{R_{sense} + R_{load}} = \frac{3.3 - 0.7}{2200 + 0} = 1.18\,mA \tag{3.28}$$

where sense resistor resistance is $R_{sense} = 2200\,\Omega$, test enable supply voltage is $U_{enable} = 3.3\,V$ and diode forward voltage is $U_D = 0.7\,V$. The maximum test current $I_{max} = 1.18\,mA$ is significantly smaller than minimum firing current of pyrotechnic charges and therefore is safe to use.

Voltage U_{cont} measured at the continuity signal output is described by equation 3.29.

$$U_{cont} = U_D + U_{R_{load}} \quad [V] \tag{3.29}$$

Based on that equation, resistance of the load can be approximated with formula 3.30, but the calculated resistance value will not be very precise since the circuit is designed for continuity detection rather than resistance measurement.

$$R_{load} = R_{sense}\frac{U_{cont} - U_D}{U_{enable} - U_{cont}} = 2200 \cdot \frac{U_{cont} - 0.7}{3.3 - U_{cont}} \quad [\Omega] \tag{3.30}$$

Low-pass filters are added to AD converter inputs formed by resistors $R44$ and $R45$ and capacitors $C53$ and $C54$. This filter acts as anti-aliasing filter and is also used to filter out higher frequency noises for more accurate measurements. Since the measured load resistance is supposed to be constant, the selected cut-off frequency f_{cutoff} of the filter is low as shown in formula 3.31.

$$f_{cutoff} = \frac{1}{2\pi RC} = \frac{1}{2\pi \cdot 10^4 \cdot 10^{-6}} \doteq 15.9\,Hz \tag{3.31}$$

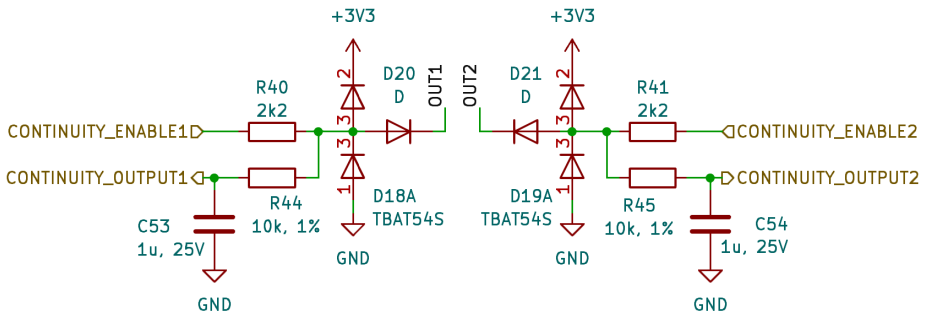

Figure 3.15: Continuity Tester Circuit on Flight Computer

3.6 Wireless Communication

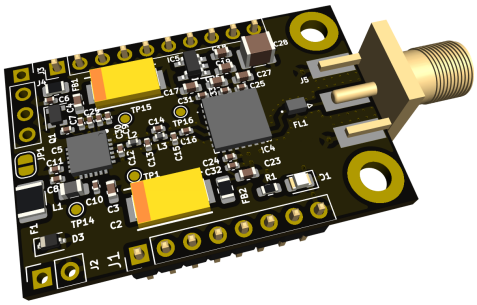

Figure 3.16: RocketLink PCB

Wireless communication is used for telemetry data transmission and remote control of the onboard avionics. For this application, a wireless communication module called "RocketLink" is used. It was designed by CTU Space Research team along with ground-based receiver and other infrastructure for control of the rocket.

The RocketLink module is an integrated solution for wireless communication. All components required for wireless transmission are part of the module along with SMA antenna connector. It features SX1280 wireless transceiver operating on $2.4\,GHz$ frequency capable of LoRa and FSK modulation. The transceiver can communicate with microcontroller through SPI or UART interface. Analog frontend and $30\,dBm$ integrated amplifier SKY65383-11 is present on the module as well.

The module is in form of a 39x24 mm daughter board that can be soldered into other boards such as the flight computer in this case. It requires up to $1\,A$ current at $3.3\,V$ during transmission with the highest power setting. The module is connected to $3.3\,V$ power rail through a ferrite bead to filter out high frequency noise. SPI bus was selected as the primary communication interface between the module and the microcontroller and the module is assigned with a dedicated SPI peripheral in the MCU. Interrupt output and other required control pins are connected to the microcontroller as well.

3.7 Connectivity

Multiple connectors are present on the flight computer that allow connection with other parts of the onboard avionics system ranging from RocketBus or USB to programming and other expansion interfaces.

3.7.1 RocketBus

Two RocketBus connectors are present on the flight computer as outlined in section 2.3.1. They are used to connect other components of onboard avionics

to the flight computer as well as to connect the battery. Wide traces are used to connect RocketBus connectors to minimize power losses.

Since CAN bus is used for communication between onboard avionics components, CAN bus transceiver $TCAN332G$ is used to interface between differential bus lines and CAN protocol controller in microcontroller. It supports data rates up to $5\,Mb/s$ and also includes support for CAN FD protocol that could be used in the future for faster data transmission.

Used circuit is shown in figure 3.17. Decoupling capacitors are added according to manufacturer recommendations. Additional bulk capacitor is also added to ensure stable power since CAN is a critical feature of the design. $120\,\Omega$ termination resistor is present on the board with solder jumper $JP4$ for simple selection of terminator position. CAN bus requires termination on both ends of the bus topology [9] and because of the modular design of onboard avionics, different configurations can result in different optimal positions of the termination resistor. Additional TVS diodes are placed near connectors to protect the board from electrostatic discharge [38].

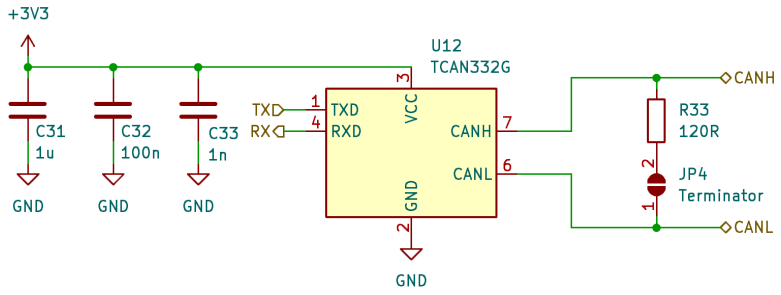

Figure 3.17: CAN Bus Transceiver Circuit

3.7.2 USB

USB C connector is added to the board for simpler connection with PC. It can be used for configuration of the flight computer as well as for download of flight data. The circuit is shown in figure 3.18. The differential data lines are connected through TVS protection diodes directly to USB Full Speed transceiver integrated in the microcontroller. Configuration Channel (CC) pins are connected through $5.1\,k\Omega$ resistors to ground for correct detection of flight computer as a power sink device [39]. USB bus power can be used for powering logic components of the flight computer to allow communication with PC without battery connected. Power from USB can be disconnected with $JP3$ jumper if necessary. Voltage on the bus power line is sensed by the microcontroller to correctly set software state machines for USB communication during connect and disconnect events.

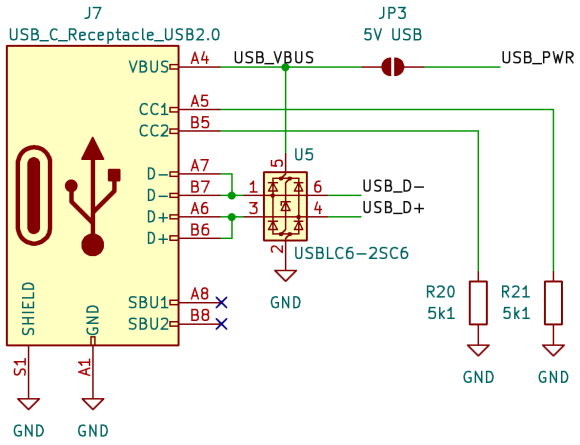

Figure 3.18: USB Interface Circuit

3.7.3 Auxillary

Additional auxillary interfaces are present on the flight computer. They can be used to connect umbilical connector to the flight computer if the rocket supports it and future expansion is also possible. For this purpose two UART interfaces are available along with SPI and I2C interface. Serial Wire Debug (SWD) interface is also present on the flight computer for programming and debug of the microcontroller. The expansion interfaces use Molex KKPLUS250 series connectors for reliable connection and each is equipped with TVS protection diodes.

3.8 Storage

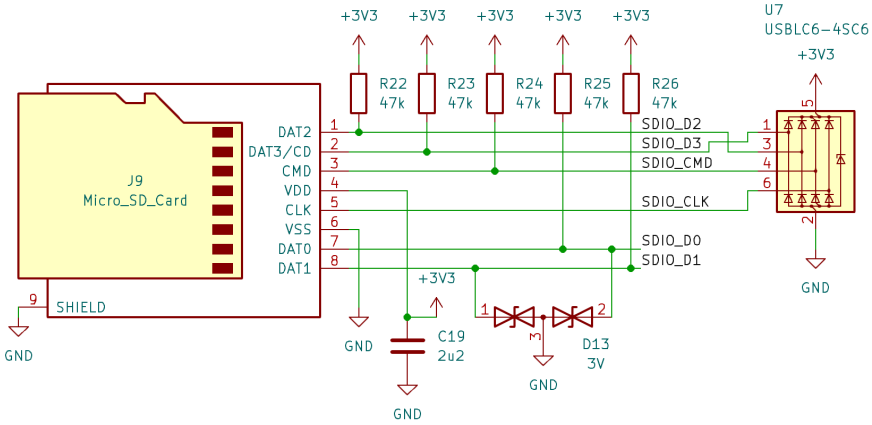

Figure 3.19: MicroSD Card Connection Circuit

For onboard storage of flight data, microSD card is used. In previous flight computers of CTU Space Research team, EEPROM memory was used for storing flight data, but it became a limiting factor due to small size and low

speed for flight data recording at high frequencies. MicroSD cards feature much higher capacity and higher speed than EEPROM memory along with ability to plug the card directly into a computer for flight data download.

MicroSD card is connected to 4-bit wide SDIO interface in the microcontroller for fast data transfer. According to manufacturer's example, pull-up resistors are connected to the data lines [40]. Bulk capacitor is added to supply current to the microSD card during write operations. TVS diodes are used to protect the microcontroller from damage that could be caused by ESD discharge. They are placed near the connector in signal path to maximize effectiveness of the protection [38]. Socket with hinged door is used to hold the microSD card in place as this type of socket can endure high acceleration conditions during flight better than push-pull or push-push socket type.

3.9 Status Indication

Status indicators are present on the flight computer. They can be used to indicate various states of the flight computer and to aid finding the rocket after landing.

3.9.1 Light Indicators

The flight computer features a simple light status indicator in form of RGB LED controlled by the microcontroller. The RGB LED can use different colors to signalize different states of the flight computer to the operators during preparations for flight. RGB LED was selected instead of multiple single-color LEDs for easier identification of the state as it can be difficult to distinguish between separate LEDs when the flight computer is installed inside rocket with difficult access.

In addition to the status RGB LED, the flight computer also features LEDs indicating presence of voltage on power lines. As was mentioned in section 3.5.2, LED indicating power outputs continuity and power outputs state are present on the flight computer as well.

3.9.2 Buzzer

When the flight computer is mounted inside the rocket, light indicators can't be seen from the outside. Buzzer can be used to indicate flight computer state by sound in this case. It can also help with localization of the rocket during recovery after landing.

Passive buzzer was selected as it can produce different frequencies of sound. The buzzer can produce sound power level up to $100\,dB$ at $4\,kHz$ [41] to aid with localization of the rocket. It is driven by N-MOSFET transistor according to a PWM signal generated by timer peripheral in the microcontroller as shown in figure 3.20. Pull-down resistor $R7$ is added to avoid floating gate of the transistor during start-up. Flyback diode $D8$ is connected to the buzzer

to suppress voltage spikes from inductive load switching. Additional bulk capacitor is connected as well to reduce noise on the power line.

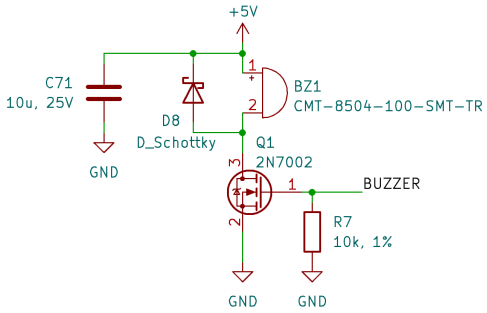

Figure 3.20: Buzzer Driver Circuit

3.10 PCB Layout

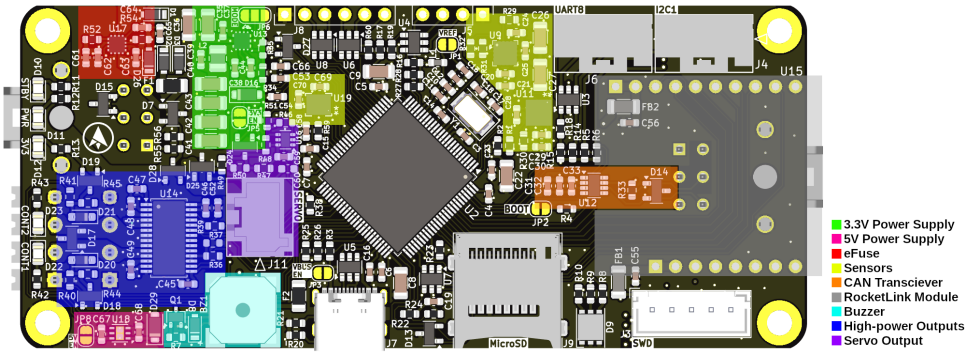

Figure 3.21: Layout diagram of the flight computer

Layout of components on the board was carefully considered to avoid interference between different parts of the circuit. Size and shape of the board was considered as well to be able to fit the flight computer inside smaller rockets. High level overview of the layout is shown in figure 3.21. Firstly, the most important parts of the circuit were placed such as power supplies, microcontroller, sensors and connectors. Then the rest of the circuit was placed. All components were laid out while taking trace routing into account and to make the board as small as possible. After all components were placed, routing of signal traces was done. Cuts in ground plane were avoided for optimal current return paths. Most of components are placed on the front side of the board to simplify assembly of the board. Majority of passive components use 0603 package as it can be easily assembled by hand.

Even though the design would benefit from 6-layer PCB, 4-layer stackup was chosen because of significantly lower manufacturing costs. The layer stackup uses the front layer as main signal routing layer with second layer as a ground plane to reduce EMI. Third layer is used for power plane and

occasional signal traces that did not fit into the front layer [38]. The bottom layer is used mostly as a ground plane for GPS receiver.

The microcontroller and its supporting components are placed in the middle of the board because majority of components are connected to the microcontroller. Decoupling capacitors are placed as close to power pins of components as possible. Sensors are located near the microcontroller to reduce length of signal traces. Magnetometer is placed away from power supplies and high current traces to minimize interference. GPS receiver is located on the back side of the board to provide clean continuous ground plane for optimal antenna performance without nearby components that could interfere with GPS signal. Right hand side of the board is reserved for RocketLink wireless module along with CAN transceiver. CAN bus traces are routed as a differential pair.

Power management circuits and actuator outputs are on the left hand side of the board and their high current traces do not cross parts of board with sensitive components. Switching power supply is carefully laid out to minimize size of current loops to reduce EMI. RocketBus connectors are placed on opposite sides of the board for easier daisy-chaining of avionics boards in the rocket. They are connected together using wide traces to minimize losses. Thermal vias connected to large copper planes are placed under and near components that might heat up to dissipate heat more effectively.

Finished board is shown in renders in figure 3.22 and 3.23. The board size is 100x44 mm with 4 mounting holes in corners. The mounting holes are designed for M3 screws and their pitch is 93x37 mm.

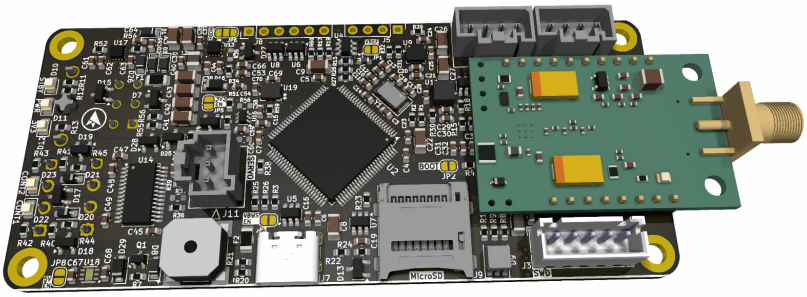

Figure 3.22: Front side of flight computer board

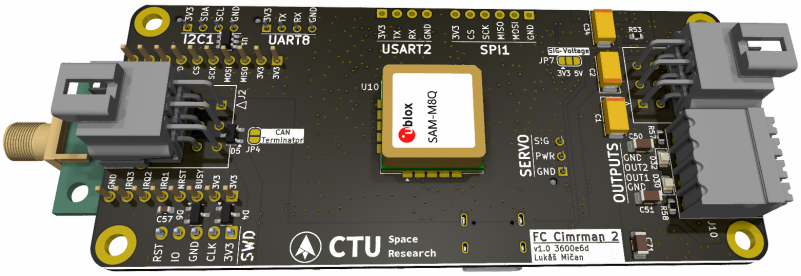

Figure 3.23: Back side of flight computer board

Chapter 4

Section Management Board Design

In this chapter the design process of the section management board is described. The section management board is a support equipment for the main flight computer enabling control of larger and more complex rockets as described in section 2.3. Similarly to the flight computer, the design uses commonly available off-the-shelf (COTS) components with components' product lifecycle taken into account to ensure the used components will not be discontinued in the near future. Automotive grade components were used where possible as well. Section management board borrows some subsystems from the flight computer to speed-up the design process.

4.1 Section Management Board Architecture

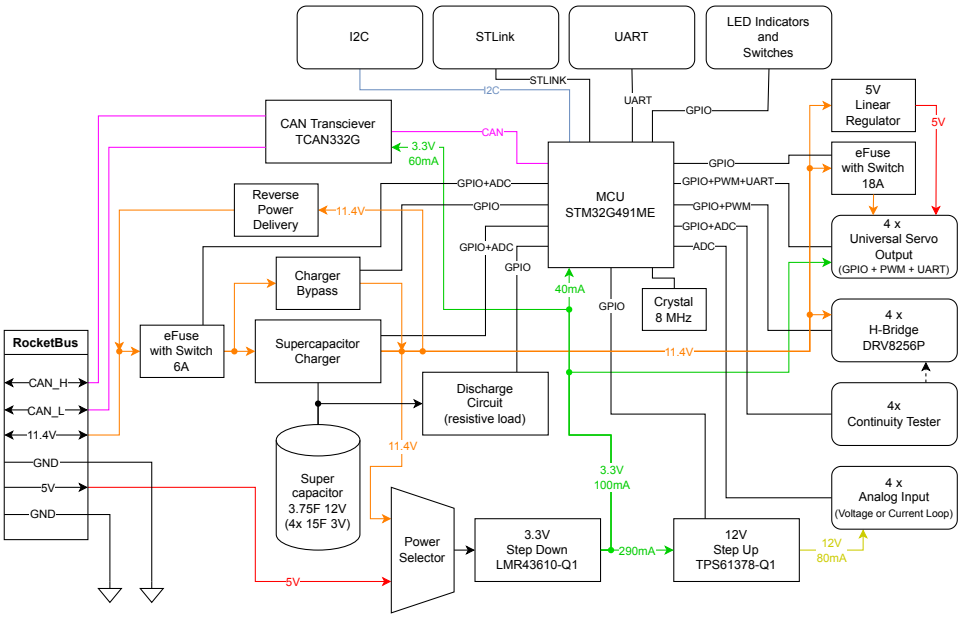

Figure 4.1: Section Management Board Block Diagram

Section Management Board diagram is shown in figure 4.1. The microcontroller (MCU) is the main processing unit responsible for all operations such as controlling all inputs and outputs and communication with main flight computer. Multiple actuator outputs for servomotor control and pyrotechnic charge ignition are available as well as external sensor inputs. LEDs are used for status indication and DIP switches are integrated into the board for simple function mode selection. In addition, serial buses UART and I2C are brought out to connectors to allow for expansion in the future.

Supercapacitors are utilized as a backup power source and to supply high-current pulses for actuator outputs. For that purpose a supercapacitor charger and discharge circuit along with electronic fuses and switches are present. Power selector automatically selects power source with the highest voltage and passes it to the logic circuits power regulator. Thus the board can operate from energy stored in the supercapacitors even when the main power supply fails. Step-up switching power supply provides stable power to external sensors.

4.2 Microcontroller

The section management board uses STM32G491ME microcontroller, because this series of microcontrollers have been used by CTU Space Research in multiple projects in the past and it fulfills the design requirements for section management board. Some already developed software components for this microcontroller series could be used as well. Software for the section management board will be written using STM32CubeIDE, however, this microcontroller is also supported by the Matlab Embedded Coder [16].

The microcontroller features ARM Cortex-M4 core that can be clocked up to $170\,MHz$ with $512\,kB$ of flash memory for program and $112\,kB$ of random-access memory [42]. Floating-point unit and DSP instructions are supported as well. STM32G491ME microcontroller uses LQFP80 package that houses enough pins for all components on the board and is easily solderable by hand.

Pin assignment is shown in figure 4.2. The assignment was done taking physical layout of components on the board into account to simplify routing of the signals. Since the section management board contains circuits mostly for interaction with external sensors and actuators, connectors positions were determined first along with their components.

Decoupling capacitors were added according to manufacturer recommendations [42] as shown in figure 4.3. Similarly to the flight computer, the analog power supply is connected through ferrite bead $L1$ to filter out high frequency noise from digital circuits and solder jumper $JP1$ can be used to select between internal voltage reference and power supply voltage reference. Since the internal oscillator circuit in the STM32G491 microcontroller is similar to microcontroller used in the flight computer with the same oscillator requirements, the same crystal and load capacitors are used.

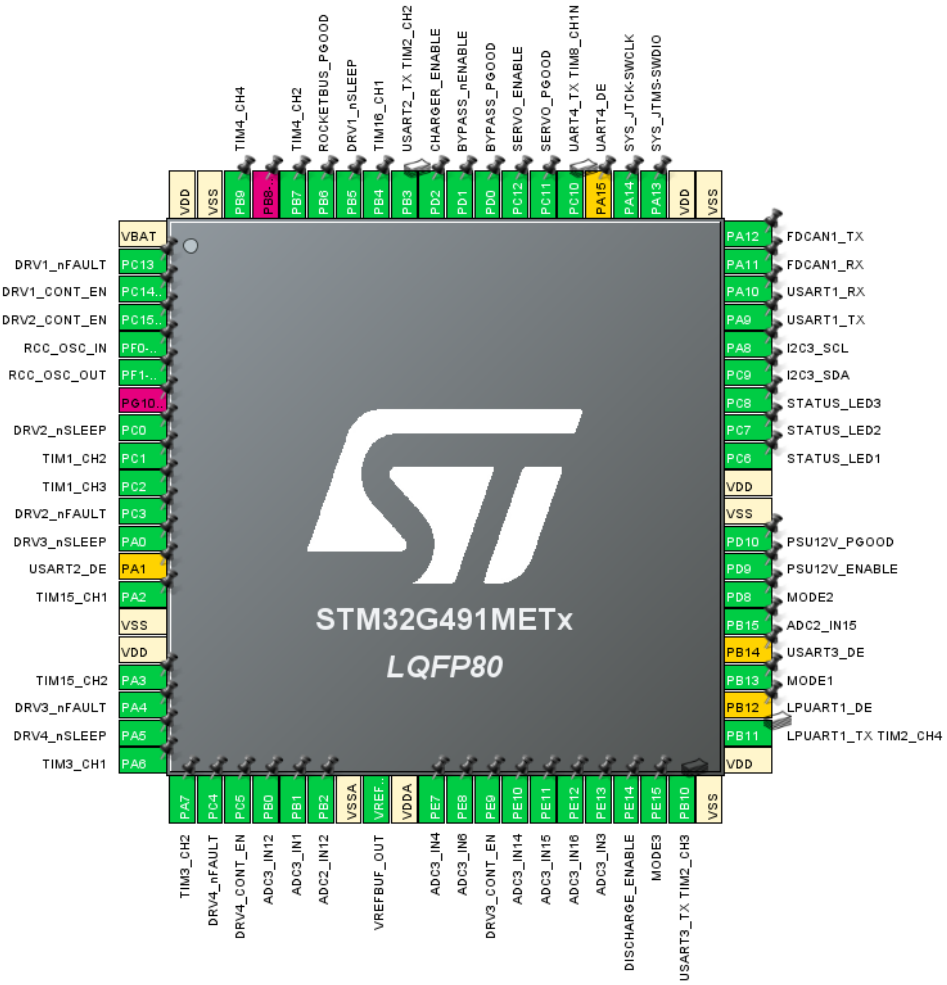

Figure 4.2: Section Management Board Microcontroller Pins Assignment

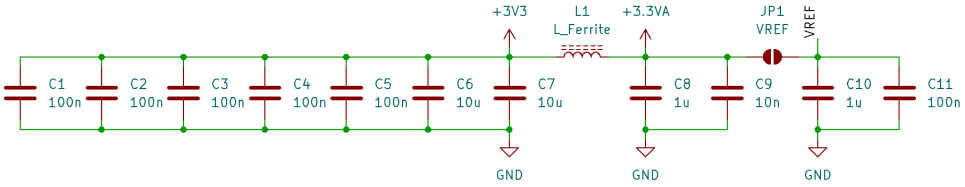

Figure 4.3: Power Supply Scheme for Section Management Board MCU

4.3 Power Management

The power management system for the section management board is shown in figure 4.4. The board is powered from RocketBus. Stand-by power line is connected to power selector to power logic components. The power selector design is the same as in the flight computer described in section 3.4.2, except only two inputs are present. High power line is connected through electronic

fuse with the same circuit design as in the flight computer described in section 3.4.1, except the enable feature is not used and the fuse is always turned on.

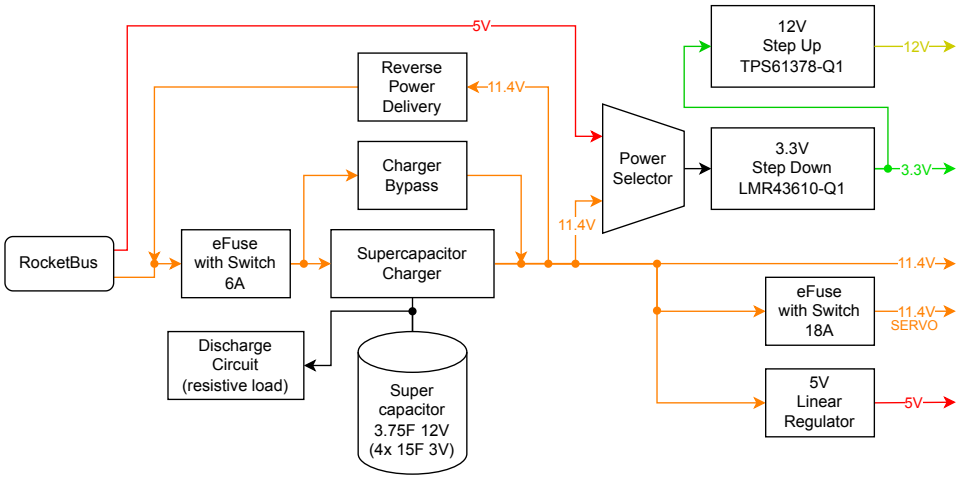

Figure 4.4: Section Management Board Power Management Diagram

Section management board is equipped with supercapacitors acting as a backup power source and they also serve as a power source for high current pulses. Supercapacitors are charged using a switching mode charger circuit. In addition, a charger bypass switch is present that can connect the high power line input directly to charged supercapacitors avoiding the supercapacitor charger. Also in cases when the supercapacitors are not connected to the board, the bypass circuit is used to supply power to the actuator outputs. Ideal diode is present to allow reverse current flow to the high power line for disarming and backup power purposes as outlined in section 2.3.3. Supercapacitors are connected to the power selector as well and thus the whole board can be powered with energy stored in the supercapacitors in case of main power failure.

Power for servo outputs is connected through electronic fuse with switch that can be used to power down servos when not used to save power. Actuator power output circuits contain integrated overcurrent protection and fuse for this purpose was not used. Logic components are supplied with 3.3V step-down switching power supply. 12V step-up switching power supply is used to power external sensors and it is powered from 3.3V power line to allow use of simpler switching structure. Voltage on the high power line can vary and if the 12V power supply would be connected directly to it, then a more complex switching structure that can convert voltage up and down would be needed. Linear 5V power supply is used to power logic components that generate signal for servo outputs. The design of the 5V power supply is shared with the flight computer and is described in section 3.4.4.

4.3.1 Supercapacitors

As described in previous paragraphs, the supercapacitors serve as a backup power source and as a high current pulse power source for actuators. To match RocketBus high power line voltage, four capacitors are used. Each capacitor can be charged up to $3\,V$ resulting in total possible charge voltage of $12\,V$. The supercapacitors were sized according to required current pulse length.

The supercapacitors are required to sustain $I = 6\,A$ current pulse with duration of $t = 1\,s$ with $\Delta U = 2\,V$ voltage drop. This may represent turning of a servomotor to close or open a valve or to release the recovery system. From equation 4.1 [43] the formula 4.2 for required supercapacitor capacity is derived.

$$\Delta Q = C \cdot \Delta U = I \cdot t \tag{4.1}$$

$$C = \frac{I \cdot t}{\Delta U} = \frac{6 \cdot 1}{2} = 3\,F \tag{4.2}$$

Capacity of at least $3\,F$ is required. Since series connection of capacitors lowers their total capacitance [43], each supercapacitor needs to have capacity of at least $4 \cdot C = 12\,F$. From available options on the market, supercapacitors with capacity $15\,F$ were selected. The total capacity of the supercapacitor stack is $\frac{15}{4} = 3.75\,F$.

Supercapacitor Charger

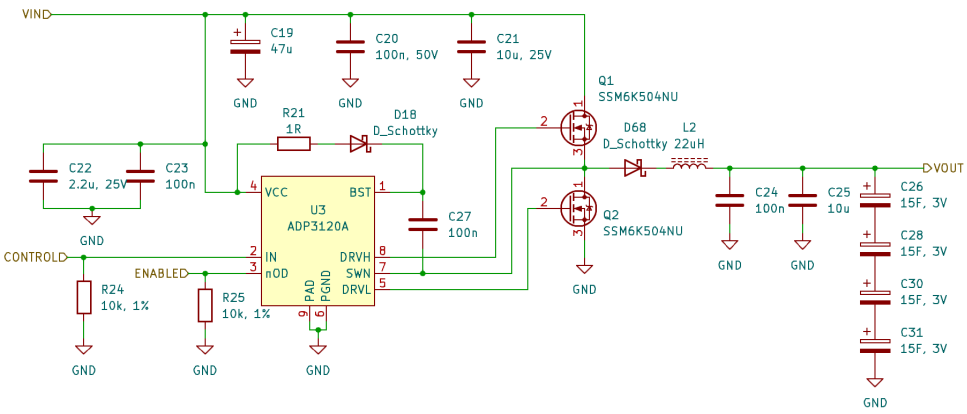

Figure 4.5: Supercapacitor Charger Circuit

The supercapacitor charger is responsible for safe and efficient charging of the supercapacitors. Switching-mode charger topology was selected because it allows faster charging with lower losses and heating compared to linear chargers [44].

Simple custom charger circuit was designed because none of the integrated solutions available on the market fulfilled the requirements for control of the charging process. The charger circuit is shown in figure 4.5. The circuit operates as a synchronous step-down converter using ADP3120A dual MOSFET

driver with current feedback control. Current flowing through the charger is measured by the main electronic fuse. Switching control signal is generated by timer peripheral in the microcontroller controlled by software. Enable signal is used to turn the charger on and off when necessary. Both inputs include pull-down resistors to disable the charger during start-up.

Inductor value was estimated using formula 4.3 [31]. Maximum duty cycle D changes according to the supercapacitor voltage and can approach $D = 1$ at the end of charging. Ripple current was set to $I_{ripple} = 0.5\,A$ and switching frequency was set to $f_{SW} = 1\,MHz$ to minimize charger footprint on the board.

$$L = \frac{(U_{in} - U_{out}) \cdot D}{f_{SW} \cdot I_{ripple}} = \frac{(12 - 0) \cdot 1}{10^6 \cdot 0.5} = 24\,\mu H \tag{4.3}$$

Inductor value $L2 = 22\,\mu H$ with saturation current $4.3\,A$ was selected as a commonly available part.

Decoupling capacitors for the MOSFET driver were added according to manufacturer recommendations [45]. The MOSFET driver uses bootstrap circuit to control high-side MOSFET. The minimum capacitance C_{bst} of the bootstrap capacitor is determined according to formula 4.4 [45]

$$C_{bst} = \frac{Q_{gate}}{dV_{bst}} = \frac{12.8 \cdot 10^{-9}}{0.3} \doteq 42.67\,nF \tag{4.4}$$

where $Q_{gate} = 12.8\,nC$ [46] is gate charge of the used transistor and $dV_{bst} = 0.3\,V$ is allowed voltage drop on the bootstrap capacitor. Bootstrap capacitor $C27 = 100\,nF$ was used.

Resistor $R21$ was added to limit peak charging current of the bootstrap capacitor within operating conditions of the bootstrap diode $D18$. The bootstrap capacitor $C27$ with resistor $R21$ form RC circuit with time constant $\tau = R21 \cdot C27 = 1 \cdot 10^{-7} = 100\,ns$. This limits the minimum off-time of the switching signal to ensure correct charging of the bootstrap capacitor, however, the calculated value is acceptable.

The selected transistors have gate resistance $R_{gate} = 8\,\Omega$ [46] and when combined with output resistance of the gate driver $R_{driver} = 2.2\,\Omega$ [45] it results in peak gate current $I_{gate} = \frac{U_{in}}{R_{driver}+R_{gate}} = \frac{12}{8+2.2} \doteq 1.18\,A$. Charging of the MOSFET gate follows time constant $\tau = (R_{gate} + R_{driver}) \cdot C_{gate} = (8 + 2.2) \cdot 1.1 \cdot 10^{-9} = 11.22\,ns$. This is acceptable for switching at frequency $f_{SW} = 1\,MHz$.

Diode $D68$ is added for protection of the circuit against backflow from the supercapacitors during control software development and it should be replaced with a short circuit after ensuring the control algorithm works correctly.

Charger Bypass

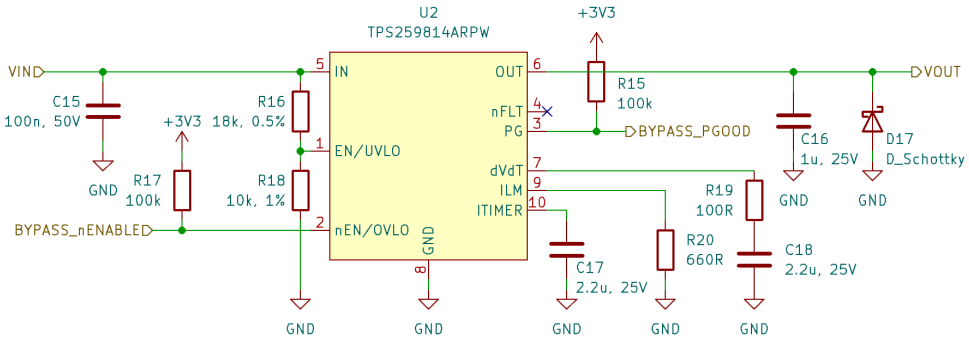

Figure 4.6: Supercapacitor Charger Bypass Circuit

Charger bypass circuit is used to allow direct connection between the high power line and the supercapacitors. This is needed for continuous supply of power from RocketBus to outputs as the charger circuit cannot be closed permanently. For this purpose, the same integrated circuit TPS25981 as the main electronic fuse is used, but with different settings as shown in figure 4.6. This electronic fuse is set up to always trigger after the main fuse to avoid nondeterministic behaviour. Maximum current is set to $I_{lim} = 10\,A$ using formula 4.5.

$$R_{ILM} = \frac{6585}{I_{lim}} = \frac{6585}{10} = 658.5\,\Omega \tag{4.5}$$

Commonly available value of resistor $R20 = 660\,\Omega$ is used instead. Current measurement functionality is not used.

Time period when double maximum current is allowed is set to $t_{ITIM} = 1.6\,s$ using formula 4.6

$$C_{ITIM} = t_{ITIM} \cdot \frac{I_{ITIM}}{dV_{ITIM}} = 1.6 \cdot \frac{2 \cdot 10^{-6}}{1.51} \doteq 2.12\,\mu F \tag{4.6}$$

where $I_{ITIM} = 2\,\mu A$ and $dV_{ITIM} = 1.51\,V$ are constant parameters of the electronic fuse. Commonly available value of capacitor $C17 = 2.2\,\mu F$ is used instead.

Inrush current control feature is important in this case, because direct connection of RocketBus to the supercapacitor might result in high current surges when operated incorrectly. RocketBus can be connected directly to the supercapacitor only after the supercapacitor is fully charged. To help mitigate high current surges when the power switch is closed and the supercapacitor voltage is close but not the same as the RocketBus voltage, the inrush current control feature is used. Inrush current limit $I_{inrush} = 5.5\,A$ for output capacity $C_{out} = 3.75\,F$ is set using formula 4.7.

$$C_{dVdt} = \frac{3.3 \cdot 10^{-6}}{SR} = \frac{3.3 \cdot 10^{-6}}{\frac{I_{inrush}}{C_{out}}} = \frac{3.3 \cdot 10^{-6}}{\frac{5.5}{3.75}} \doteq 2.25\,\mu F \tag{4.7}$$

Commonly available value of capacitor $C18 = 2.2\,\mu F$ is used instead. According to manufacturer recommendations, current limiting resistor $R19$ is added because of large capacitor $C18$. This setting results in long start time $t = \frac{U_C}{SR} = \frac{12}{1.467} \doteq 8.18\,s$.

In this case the EN/UVLO pin is not used to control the power switch, because it activates quick output discharge feature that attempts to discharge the output where supercapacitor is connected. Instead nEN/OVLO pin is used for this purpose. It is equipped with pull-up resistor to keep the power switch open during microcontroller start-up. Power good signal indicating state of the fuse is connected to the microcontroller.

Supercapacitor Discharge and Measurement

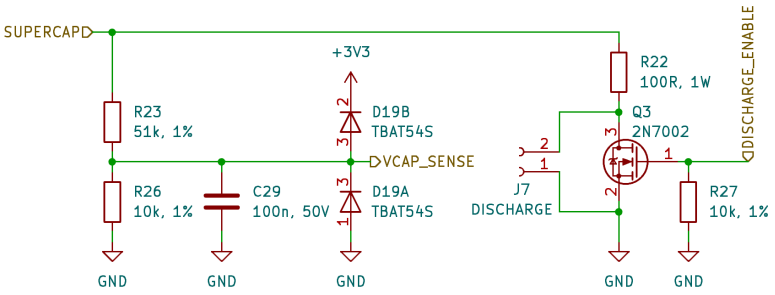

Figure 4.7: Supercapacitor Discharge and Measurement Circuit

Circuit shown in figure 4.7 is used for supercapacitor discharging and measurement of supercapacitor voltage. Discharging is handled by dissipating stored energy into heat using resistive load. The discharging process is controlled by N-MOSFET transistor. In addition, pin header is provided to allow discharging of the supercapacitor without microcontroller intervention. Resistor $R22$ used for energy dissipation limits maximum discharge current. Using $R_d = 100\,\Omega$ resistor to discharge supercapacitor charged to $U_C = 12\,V$ results in peak current $I_d = \frac{U_C}{R_d} = \frac{12}{100} = 0.12\,A$ and peak power $P_d = U_C \cdot I_d = 12 \cdot 0.12 = 1.44\,W$. For this purpose, a high wattage resistor is soldered to a large copper plane with thermal vias to help dissipate heat.

The supercapacitor with capacity $C = 3.75\,F$ and resistor R_d form RC circuit with time constant $\tau = R_d C = 100 \cdot 3.75 = 375\,s$. Thus discharging of the supercapacitor through this circuit takes fairly long time and the discharge speed is limited by slow heat dissipation. For faster discharging of the supercapacitor, external resistor is used along with reverse power delivery circuit.

For supercapacitor voltage measurement, a resistive voltage divider is used and its output is measured with AD converter in the microcontroller. Series diodes $D19$ provide overvoltage protection for the AD converter. Real supercapacitor voltage U_C can be calculated from measured voltage U_{meas} with formula 4.8.

$$U_C = U_{meas} \cdot \frac{R23 + R26}{R26} = \frac{61}{10} U_{meas} \quad [V] \tag{4.8}$$

Divider output is equipped with anti-aliasing low-pass RC filter with cutoff frequency f_{cutoff} calculated using formula 4.9.

$$f_{cutoff} = \frac{1}{2\pi \cdot R23 \| R26 \cdot C29} = \frac{1}{2\pi \cdot \frac{51 \cdot 10^3 \cdot 10^4}{51 \cdot 10^3 + 10^4} \cdot 10^{-7}} \doteq 190.4\,Hz \qquad (4.9)$$

4.3.2 Reverse Power Delivery

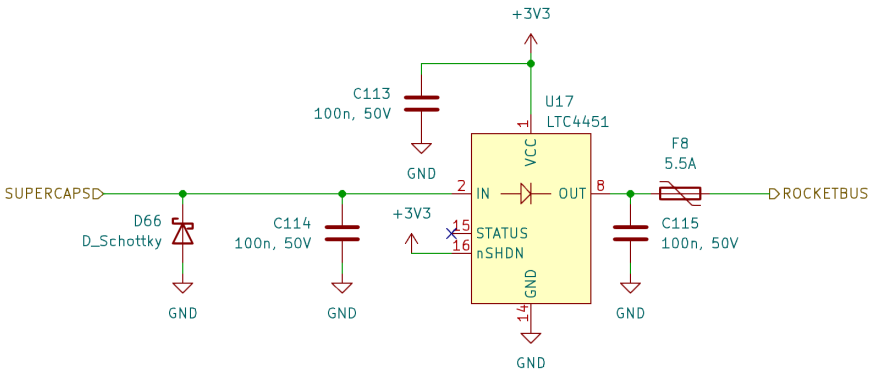

Figure 4.8: Reverse Power Delivery Circuit

Reverse power delivery circuit is used to supply power from supercapacitors back to RocketBus to power other components in case of main power failure. Simultaneously it is used to discharge the supercapacitors when arming pin is inserted as described in section 2.3.3. The circuit uses ideal diode to minimize heat losses, because currents up to $5\,A$ could be flowing there and classical or Schottky diodes would emit too much heat. Additional resettable PTC fuse is used to protect the ideal diode from overcurrent.

Fully integrated ideal diode LTC4451 is used for this purpose. The circuit is shown in figure 4.8. Decoupling capacitors are added according to manufacturer recommendations [47]. Active-low shutdown control pin is connected to $3.3\,V$ to enable the diode. Status output signal is not used. Negative spikes caused by parasitic impedance of the traces during integrated transistor switching are clamped by diode $D66$.

PCB layout of the reverse current delivery circuit is based on manufacturer recommended layout including thermal vias to help dissipate heat. Manufacturer claims that when using the recommended layout, temperature rise of $25\,°C$ is expected when $6\,A$ current flows through the circuit [47].

4.3.3 Electronic Fuse for Servo Outputs

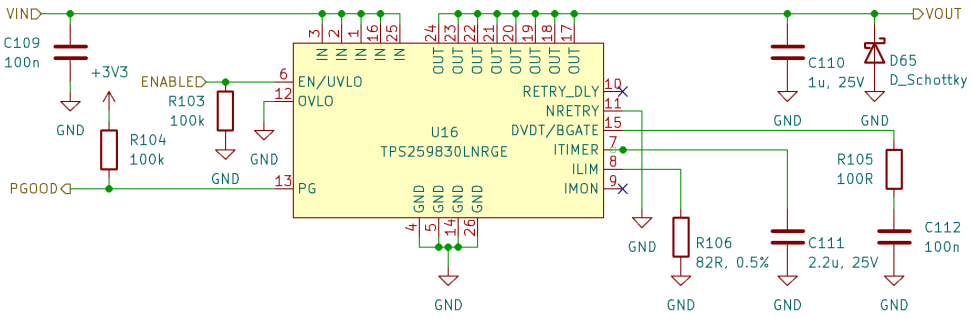

Figure 4.9: Electronic Fuse for Servo Outputs Circuit

Electronic fuse is used to protect the board from short circuit since the supercapacitor output is accessible in the servo output connector and the supercapacitor can deliver damaging amount of energy. In addition the power switch integrated in the electronic fuse can be used to disable servomotors when they are not being used to lower power consumption. For this purpose an electronic fuse TPS259830 with higher current rating is used. The circuit is shown in figure 4.9. Current limit $I_{limit} = 18\,A$ is set by resistor $R106$ calculated using formula 4.10 [48].

$$R106 = \frac{1460}{I_{limit} - 0.11} = \frac{1460}{18 - 0.11} \doteq 81.6\,\Omega \tag{4.10}$$

Resistor with value $R106 = 82\,\Omega$ was used as a close approximation.

Time period when double maximum current is allowed is set to $t_{ITIM} = 1\,s$ using formula 4.11 [48]

$$C_{ITIM} = t_{ITIM} \cdot \frac{I_{ITIM}}{dV_{ITIM}} = 1 \cdot \frac{2.1 \cdot 10^{-6}}{0.98} \doteq 2.14\,\mu F \tag{4.11}$$

Capacitor $C111 = 2.2\,\mu F$ was used instead.

Inrush current control feature is not used in this case, nevertheless, components for inrush current control setting were added to the circuit to allow simple modification in the future if needed. Commonly available component values were used resulting in output slew rate $SR = \frac{4.6 \cdot 10^{-6}}{C_{dV\,dt}} = \frac{4.6 \cdot 10^{-6}}{10^{-7}} = 46\,V/s$ [48].

The electronic fuse allows configuration of behaviour after overcurrent event. Pin RETRY_DLY is left disconnected and pin NRETRY is connected to ground. This sets the fuse to automatically retry enabling output indefinitely with minimum delay between retries. EN/UVLO pin is connected to the microcontroller to control the power switch. Pull-down resistor is added to keep the power switch disabled during microcontroller start-up. Power good signal output is connected to the microcontroller to monitor electronic fuse state.

4.3.4 3.3V Switching Power Supply

The 3.3V power supply uses similar design as the 3.3V power supply in the flight computer. The main difference is the use of 1 A variant of the converter integrated circuit LMR43610, since the section management board uses less current with maximum of 0.6 A. Many parts of the circuit such as input and output capacitors, mode selection solder jumper and feedback resistor network are the same as in the flight computer. The power supply circuit is shown in figure 4.10.

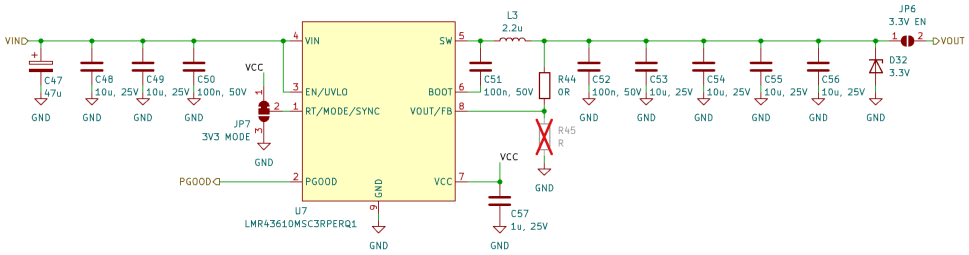

Figure 4.10: 3.3V Switching Power Supply Circuit for Section Management Board

The main difference is design for lower output current. Therefore the inductor calculations were done again using the same method. Input voltage can be in range of 4.5 V to 12 V. Firstly, preliminary inductor values for both voltage extremes were determined using formula 3.18.

$$L_{12V} = \frac{12 - 3.3}{2.2 \cdot 10^6 \cdot 0.3 \cdot 1} \cdot \frac{3.3}{12} \doteq 3.63\,\mu H \tag{4.12}$$

$$L_{4.5V} = \frac{4.5 - 3.3}{2.2 \cdot 10^6 \cdot 0.3 \cdot 1} \cdot \frac{3.3}{4.5} \doteq 1.33\,\mu H \tag{4.13}$$

Then the maximum duty cycle D was calculated with formula 3.21.

$$D_{12V} = \frac{3.3}{12 \cdot 0.85} \doteq 0.324 \tag{4.14}$$

$$D_{4.5V} = \frac{3.3}{4.5 \cdot 0.85} \doteq 0.863 \tag{4.15}$$

Based on the duty cycle and inductor values the ripple current was calculated with formula 3.24. Calculated results are in table 4.1. Current ripple with inductance $L = 3.63\,\mu H$ approaches minimal value of 0.1 A for correct operation of converter's control circuit, while current ripple with inductance $L = 1.33\,\mu H$ approaches switching transistor peak current limit. Therefore, a compromise between the two solutions was chosen and calculated values for inductor with inductance $L = 2.2\,\mu H$ are in table 4.1 as well. This solution produces current ripple that fits well into the range required by the converter across whole input voltage range. Inductor with saturation current 2.8 A was used to ensure correct operation.

U_{in} $[V]$	L $[\mu H]$	D $[-]$	I_{ripple} $[A]$
4.5	3.63	0.863	0.13
4.5	1.33	0.863	0.35
12	3.63	0.324	0.35
12	1.33	0.324	0.96
4.5	2.2	0.863	0.21
12	2.2	0.324	0.58

Table 4.1: Calculated current ripple for 3.3V SMB power supply

4.3.5 12V Switching Power Supply

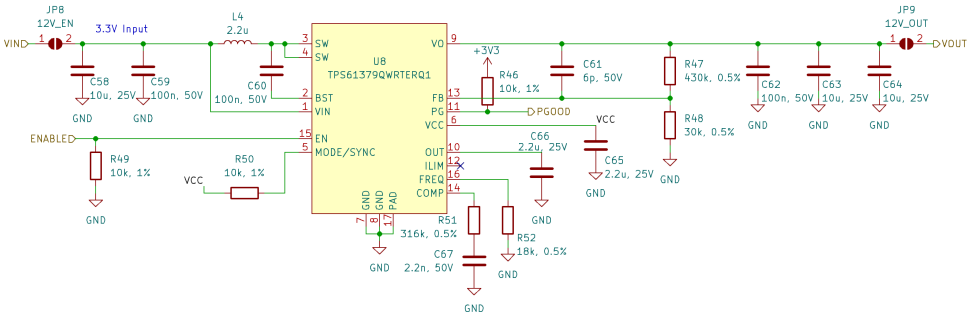

Figure 4.11: 12V Switching Power Supply Circuit for Section Management Board

12V power is required for external sensors. This is provided using a synchronous step-up converter TPS61379-Q1. It features integrated switching transistors with configurable output voltage and switching frequency in small footprint. Similarly to the 3.3V power supply, the converter uses spread-spectrum frequency modulation to reduce electromagnetic interference. It also includes output short circuit and thermal shutdown protections.

The converter circuit is shown in figure 4.11. In this design the converter operates with fixed input and output voltage resulting in simpler design process than for the 3.3V power supply. Thus converter design calculations were done using a calculator spreadsheet provided by the manufacturer [49]. Each current loop sensor requires maximum current of $25\,mA$. Four sensors can be connected to the board resulting in $100\,mA$ total current.

The converter was designed for $3.3\,V$ input voltage and $12\,V$ output voltage with maximum output current of $200\,mA$. Switching frequency $f_{SW} = 2.2\,MHz$ was selected matching the switching frequency of the 3.3V power supply. The switching frequency is set with resistor $R52 = 18\,k\Omega$. Inductor ripple current was selected to be $0.5\,A$. Using these values, the recommended inductance value was calculated to be $2.29\,\mu H$ and commonly available value $L4 = 2.2\,\mu H$ was used in the circuit as a close approximation. Inductor with high saturation current $2.8\,A$ is used to ensure correct operation of the converter.

For output voltage ripple lower than $10\,mVpp$, output capacitance larger

than 7.15 μF is required. Thus two 10 μF ceramic capacitors are used with additional 100 nF capacitor to suppress voltage spikes. Larger output capacitance improves transient load response. For input voltage ripple lower than 10 $mVpp$, input capacitance larger than 5.91 μF is required. 10 μF input ceramic capacitor is used along with 100 nF input capacitor for converter's control circuits decoupling.

Output voltage 12 V is set using a feedback voltage divider. Values $R47 =$ 470 $k\Omega$ and $R48 =$ 30 $k\Omega$ were calculated. The converter requires external control loop compensation network. Calculations were done based on target crossover frequency 20 kHz. Resulting compensation network has values $R51 =$ 316 $k\Omega$ and $C67 =$ 2.2 nF with additional feed forward capacitor $C61 =$ 6 pF.

Using this design, the calculated efficiency of the power supply is 87.5% and estimated temperature rise under load is 8 $°C$. Thermal vias connected to a large copper plane are placed under the converter to help dissipate heat. Enable control pin is connected to the microcontroller to allow turning the power supply on and off. Power good output is connected to the microcontroller as well to signalize status of the power output.

4.4 Sensor Inputs

Section management board provides four inputs for measurement of external sensor signals. The sensors can measure physical properties like temperature or pressure of the propulsion rocket subsystem. As described by requirements in section 2.1, the inputs are capable of measuring current loop signal and voltage signal.

The sensor input circuit is shown in figure 4.12. Sensors can be provided with power with user selectable voltage 12 V or 3.3 V depending on solder jumper setting. Output voltage for each sensor input can be selected individually. Output power is provided through resettable PTC fuse that protects the power supply against short circuit. Each output is protected individually, hence in case of short circuit failure of single sensor, other sensors are not affected. TVS diodes to protect against electrostatic discharge are present as well. Sensor inputs use Molex KKPLUS250 connectors as outlined in section 2.3.1.

Current loop sensors use current flowing through them to transmit sensor signal. Range of 4-20 mA is usually used and thus fault states can be easily detected when measured current is out of the specified range. Current loop is dominant standard in many industries and sensors for this standard are widely available [50].

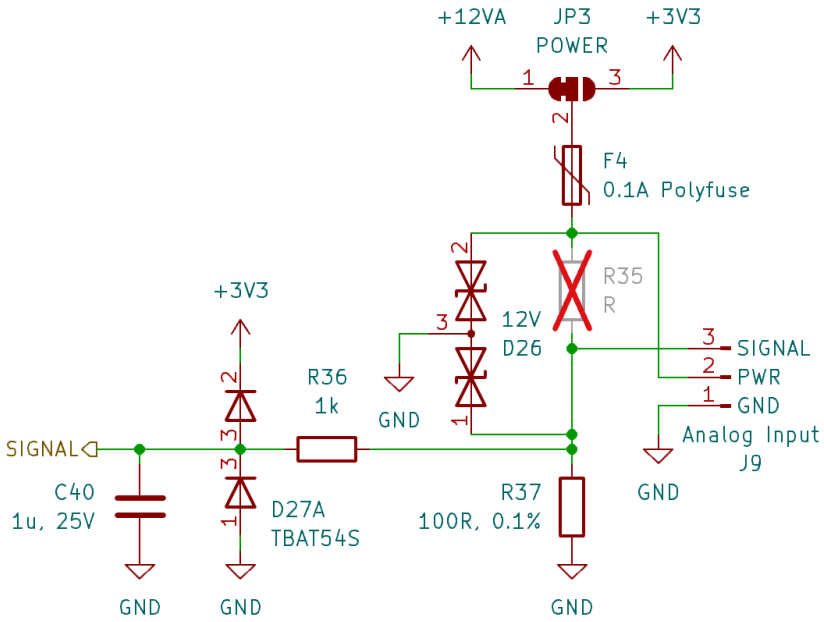

Figure 4.12: Sensor Input Circuit

In the default settings the sensor input is configured for current loop sensors with $12\,V$ output voltage and precise $R_{sense} = 100\,\Omega$ sense resistor, because all sensors used by CTU Space Research use current loop output at the moment. Value $R_{sense} = 100\,\Omega$ was selected because it nicely converts current in range 4-20 mA to optimal voltage range 0.4-2 V for the AD converter. To calculate current I_{sensor} from measured voltage U_{meas}, the formula 4.16 can be used. Conversion from measured current I_{sensor} to sensor physical quantities depends on sensor type.

$$I_{sensor} = \frac{U_{meas}}{R_{sense}} = \frac{U_{meas}}{100} \quad [A] \tag{4.16}$$

Sensor inputs are provided with anti-aliasing low-pass RC filter with cutoff frequency f_{cutoff} calculated with formula 4.17.

$$f_{cutoff} = \frac{1}{2\pi \cdot RC} = \frac{1}{2\pi \cdot 10^{3} \cdot 10^{-6}} = 159.2\,Hz \tag{4.17}$$

Protection from overvoltage of ADC input is provided by series diodes $D27$ with current limiting resistor $R36$. This setup prevents damage of the ADC input even when $12\,V$ is directly applied to the input, but it can also affect the measurement due to diode reverse leakage current. Used protection diodes have reverse current of $I_r = 0.3\,\mu A$ at $25\,°C$ ambient temperature and $I_{r_{max}} = 20\,\mu A$ at $85\,°C$ ambient temperature. Voltage drop on the current limiting resistor in the worst case is calculated with formula 4.18.

$$U_{drop} = I_r \cdot R_{limit} \quad [V] \tag{4.18}$$

$$U_{drop_{normal}} = I_r \cdot R_{limit} = 0.3 \cdot 10^{-6} \cdot 1000 = 0.3\,mV \tag{4.19}$$

$$U_{drop_{max}} = I_{r_{max}} \cdot R_{limit} = 20 \cdot 10^{-6} \cdot 1000 = 20\,mV \tag{4.20}$$

This results in negligible $0.015\%\,FS$ error in normal conditions, but $1\%\,FS$ error in the worst conditions. However, error of used sensors [51] is comparable with measurement circuit error in the worst conditions and thus it was deemed to be acceptable. Input current I_{ADC} to the ADC due to sampling capacitor charging was also considered, but it is much lower than the diode reverse leakage current as shown in formula 4.21

$$I_{ADC} = C \cdot U \cdot f = 5 \cdot 10^{-12} \cdot 3.3 \cdot 1000 = 16.5\,nA \tag{4.21}$$

where $C = 5\,pF$ is capacitance of the sampling capacitor, $U = 3.3\,V$ is the input voltage and $f = 1000\,Hz$ is the sampling frequency.

The sensor input can be configured to measure sensors with voltage output as well. Various combinations of resistors $R35$ and $R37$ result in circuits optimal for different sensor types such as platinum or NTC temperature sensors or potentiometers for position measurement. It is up to the user to determine correct configuration of those resistors based on the sensor type.

4.5 Actuator Outputs

Actuator outputs share most of the design with the flight computer described in section 3.5. Section management board features four instances of servo output circuit as well as four instances of power output circuit to allow control of more actuators.

The main difference is that H-bridges in power output circuits are each dedicated to a single actuator. They are not shared to power two unipolar actuators like power outputs in flight computer. For this purpose, Molex KKPLUS250 connectors are used for more reliable connection instead of push-button terminals.

Since the power outputs use dedicated H-bridges, different continuity tester circuit has to be used. The used circuit is shown in figure 4.13. Similarly to the continuity tester in flight computer, it also uses current flow through the load to determine continuity state. The current flows from microcontroller pin through current limiting resistor $R32 = R_{limit} = 2.2\,k\Omega$ and though diode $D25$ to the load. On the other side of the load the current flows through sense resistor $R34 = R_{sense} = 4.7\,k\Omega$ to ground. The voltage drop on the sense resistor is measured with AD converter in the microcontroller and it is used to determine continuity state. Diode $D25$ prevents current flow into the microcontroller when power output is activated. Series diodes $D23$ and $D24$ protect microcontroller from high voltage present at power output. Maximum current flowing through the load when load resistance $R_{load} = 0\,\Omega$ can be calculated using formula 4.22.

$$I_{max} = \frac{U_{enable} - U_D}{R_{limit} + R_{sense} + R_{load}} = \frac{3.3 - 0.7}{2200 + 0 + 4700} \doteq 0.38\,mA \tag{4.22}$$

Maximum current flowing through the load $I_{max} = 0.38\,mA$ is significantly smaller than minimum firing current of pyrotechnic charges and therefore is safe to use.

Voltage U_{cont} measured at the continuity signal output is described by equation 4.23

$$U_{cont} = I \cdot R_{sense} \quad [V] \tag{4.23}$$

where I is the current flowing through the load. Using this equation, the formula 4.24 for load resistance estimation can be obtained. However, the calculated resistance value will not be very precise since the circuit is designed for continuity detection rather than resistance measurement.

$$R_{load} = R_{sense} \cdot \left(\frac{U_{enable} - U_D}{U_{cont}} - 1 \right) - R_{limit} \quad [\Omega] \tag{4.24}$$

The continuity measurement output is connected to anti-aliasing low-pass RC filter with cutoff frequency f_{cutoff}. Resistor $R33$ in the filter acts also as a current limiting resistor and with diode $D24$ forms a protection circuit for the microcontroller.

$$f_{cutoff} = \frac{1}{2\pi \cdot RC} = \frac{1}{2\pi \cdot 10^4 \cdot 10^{-6}} = 15.9\,Hz \tag{4.25}$$

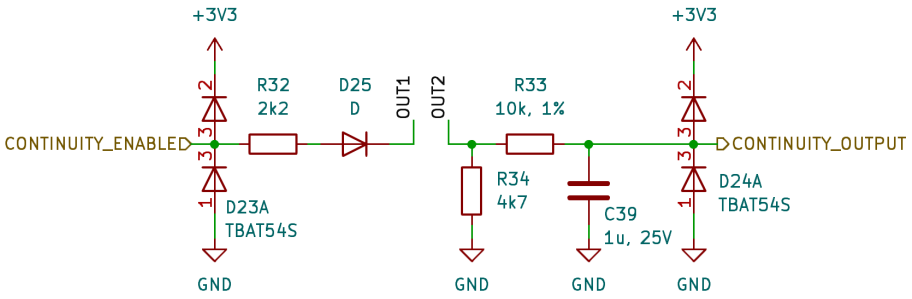

Figure 4.13: Continuity Tester Circuit on Section Management Board

4.6 Connectivity

The section management board is equipped with two RocketBus connectors for communication with other components of onboard avionics. CAN bus used for data transmission between boards uses the same circuit as the flight computer described in section 3.7.1. TVS protection diodes are present as well.

Additional UART and I2C interfaces are available for possible future expansion of the system and they use the same Molex KKPLUS250 series connectors as the flight computer. Serial Wire Debug (SWD) interface is also present on the section management board for programming and debug of the microcontroller. TVS diodes for protection against electrostatic discharge are present on all connectors.

4.7 Status Indication and Configuration

For indication of the state of the section management board, an RGB LED is used similarly to the flight computer. It helps to distinguish between states more easily compared to multiple single-color LEDs.

Simple configuration of the section management board can be using three DIP switches present on the board with circuit shown in figure 4.14. With this feature, the software in each section management board can be the same and function of the board can be selected with the switches. Software reads the state of the switches at startup and configures itself to fulfill correct tasks, since section management boards need to perform different tasks in different rocket sections. The switches are provided with pull-up resistors and TVS protection diodes to prevent damage from electrostatic discharge.

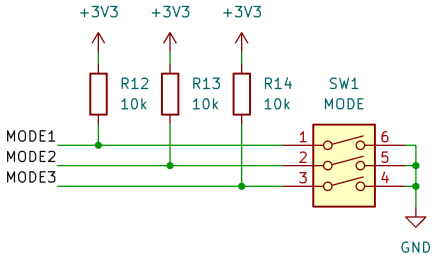

Figure 4.14: Mode Configuration Switches Circuit

4.8 PCB Layout

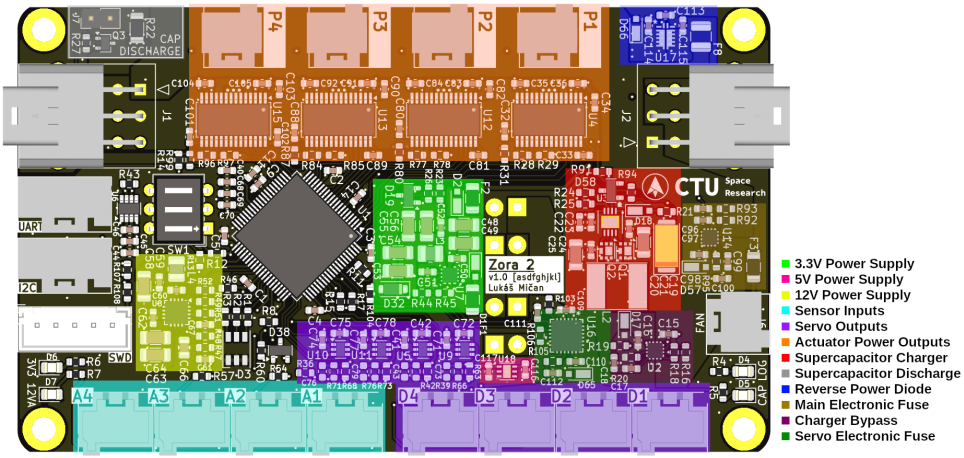

Figure 4.15: Layout diagram of the section management board

Layout of components on the board was done taking power trace routing into account, since multiple traces carrying high current are present in the circuit. Thick traces and copper pours are used to minimize their resistance. Ground plane for high power components and sensitive digital circuits is partially

separated to avoid high current flowing near sensitive components. Front and back layers are used for signal routing and for hight power traces because these layers use thicker copper compared to inner layers. The second layer is used as a ground plane and the third layer is used for power plane [38].

High level overview of the layout is shown in figure 4.15. Microcontroller is located in the middle of the board, closely surrounded by components that need a lot of connections to the microcontroller to simplify routing. Supercapacitor management circuits and electronic fuses are placed on the right side of the board away from the microcontroller and sensor inputs. Actuator power outputs and servo outputs are placed near supercapacitors to minimize trace length. All switching power supplies are laid out focusing on minimization of current loops to reduce EMI. RocketBus connectors are placed on opposite sides of the board for easier daisy-chaining of avionics boards in the rocket. CAN bus traces are routed as a differential pair. Thermal vias are placed near power components to help with heat dissipation.

Finished board is shown in renders in figures 4.16 and 4.17. The board size is 100x60 mm with 4 mounting holes in corners. The mounting holes are designed for M3 screws and their pitch is 93x53 mm.

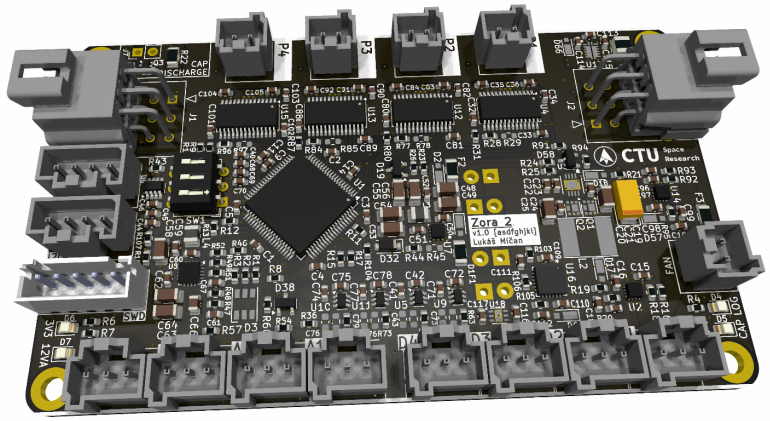

Figure 4.16: Front side of section management board

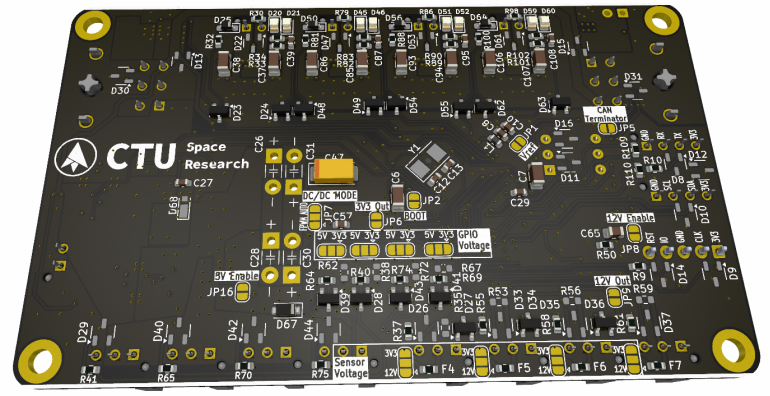

Figure 4.17: Back side of section management board

Chapter 5

Boards Realization and Testing

5.1 Realization

After the design of both boards was complete, the printed circuit boards were manufactured. SMT component assembly was done by hand using solder paste applied with stencil and soldered in a reflow oven. After all SMT components were assembled, THT components were soldered using a soldering iron. Assembled boards are shown in figures 5.1 and 5.2.

Next, the bring-up procedure was performed. Preliminary testing of power supplies one by one prevents damage to the rest of the components. Only after each power supply is checked, the solder jumpers are bridged to power the rest of the board. The bring-up procedure ended with downloading a test firmware to the microcontroller to blink an LED. This ensures that microcontroller can be programmed and more in-depth testing can follow.

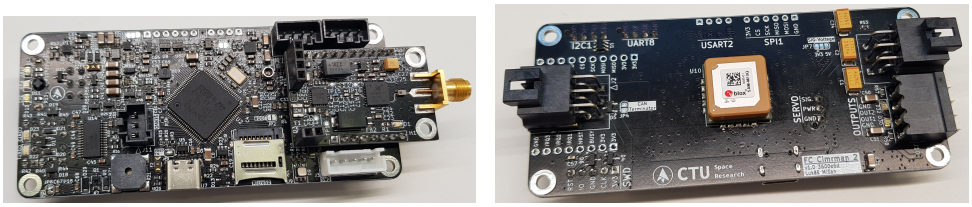

(a) : Front Side **(b) :** Back Side

Figure 5.1: Assembled Flight Computer

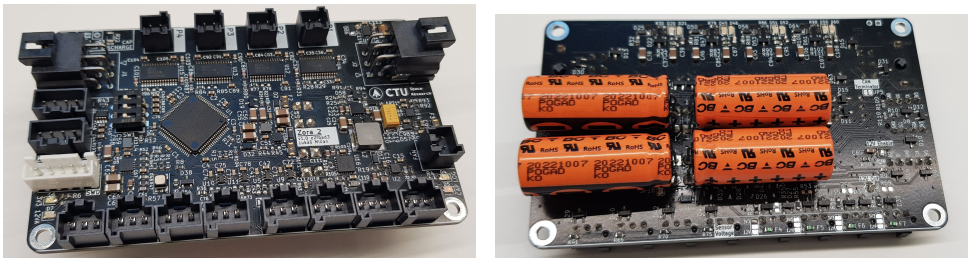

(a) : Front Side **(b) :** Back Side

Figure 5.2: Assembled Section Management Board

5.2 Testing

5.2.1 Power Management

Switching power supplies were tested under various conditions. 3.3V power supplies on flight computer and on section management board were tested with low and high load and with different input voltages. Input voltages $5\,V$ and $11.4\,V$ were tested as these are typical operating voltages of RocketBus. Power supply efficiency was calculated from measured values. Output voltage ripple under various conditions was measured as well. No overheating issues were encountered during testing. Electronic fuse control and current readout using the microcontroller works correctly. Current $3.36\,A$ was measured when $3.41\,A$ was flowing in reality. Linear 5V power supply works correctly as well.

3.3V Power Supply on Flight Computer

Test results of 3.3V power supply on flight computer are shown in table 5.1, where U_{in} is board input voltage, U_{psu} is power supply input voltage after power selector, U_{out} is power supply output voltage, I_{in} and I_{out} are input and output currents. Power conversion efficiency was calculated for the power supply itself (η) and for the whole power chain including the power selector (η_d).

The power supply behaves well in all tested conditions. Output voltage is stable under different load and input voltage combinations. Light load power conversion efficiency is low, but this is an expected effect of using FPWM power supply mode. High load power conversion efficiency is much better reaching up to $\eta = 93.9\%$ with $U_{in} = 5.06\,V$ input voltage. Losses in the power selector reduce the overall power conversion efficiency η_d but this is expected. Output voltage ripple under light load is lower than under high load as shown in figures 5.3 and 5.4.

U_{in} [V]	U_{psu} [V]	U_{out} [V]	I_{in} [A]	I_{out} [A]	η [%]	η_d [%]
5.060	4.750	3.310	0.034	0.027	**56.5**	**53.0**
5.060	4.510	3.308	0.600	0.768	**93.9**	**83.7**
11.390	11.100	3.311	0.027	0.028	**30.9**	**30.1**
11.360	10.990	3.311	0.256	0.741	**87.2**	**84.4**

Table 5.1: 3.3V FC Power Supply Test Results

3.3V Power Supply on Section Management Board

Test results of 3.3V power supply on section management board are shown in table 5.2. It behaves similarly to the 3.3V power in the flight computer, which is expected since it uses nearly the same design. Measured output voltage ripple is shown in figures 5.5 and 5.6.

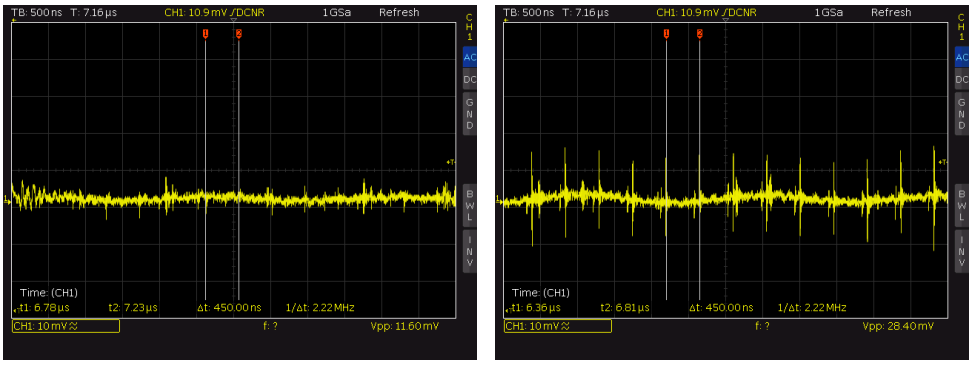

(a) : Minimal load **(b) :** High load

Figure 5.3: Output voltage ripple of 3.3V FC power supply with 5V input voltage

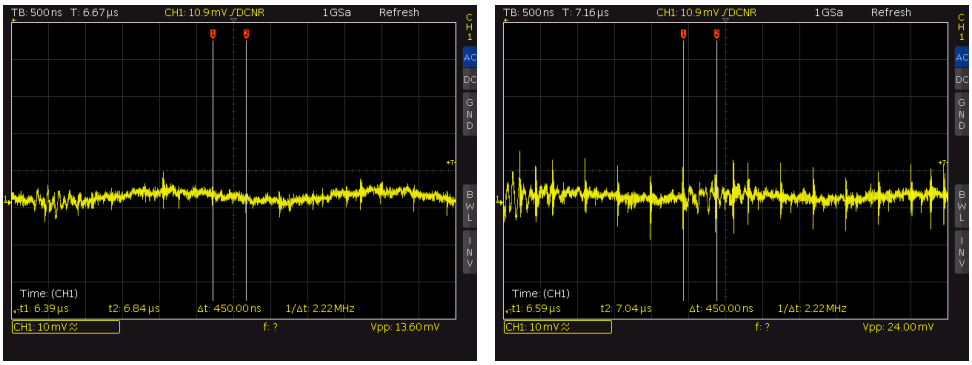

(a) : Minimal load **(b) :** High load

Figure 5.4: Output voltage ripple of 3.3V FC power supply with 11.4V input voltage

U_{in} [V]	U_{psu} [V]	U_{out} [V]	I_{in} [A]	I_{out} [A]	η [%]	η_d [%]
4.970	4.640	3.312	0.063	0.065	**73.6**	**68.8**
5.070	4.570	3.312	0.580	0.743	**92.8**	**83.7**
11.350	11.050	3.313	0.038	0.065	**51.3**	**49.9**
11.390	10.980	3.311	0.256	0.739	**87.0**	**83.9**

Table 5.2: 3.3V SMB Power Supply Test Results

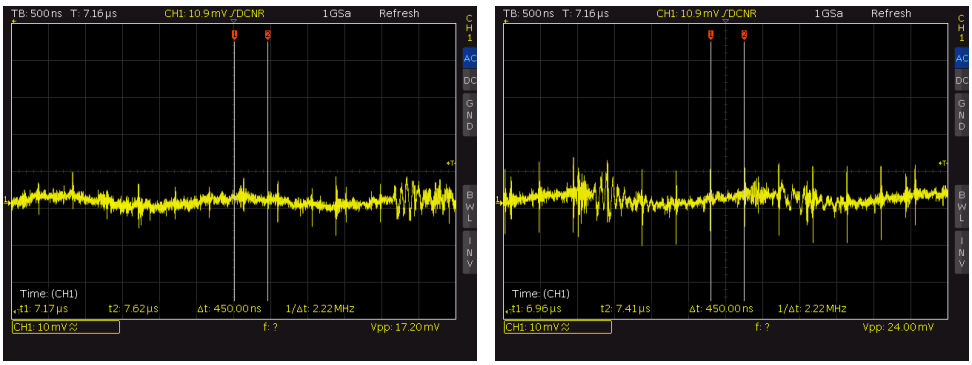

(a) : Minimal load **(b) :** High load

Figure 5.5: Output voltage ripple of 3.3V SMB power supply with 5V input voltage

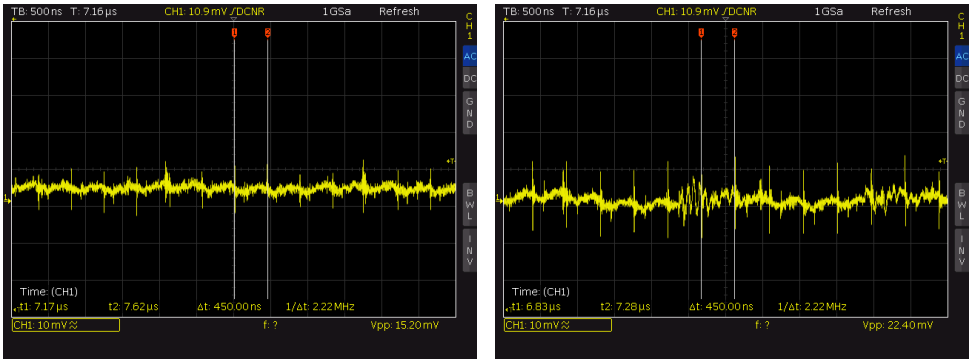

(a) : Minimal load **(b) :** High load

Figure 5.6: Output voltage ripple of 3.3V SMB power supply with 11.4V input voltage

12V Power Supply on Section Management Board

The 12V power supply on section management board does not behave as well as the 3.3V power supply. Low power conversion efficiency η under light load is expected due to the use of FPWM power supply mode, but the efficiency is fairly low even under high load as shown in table 5.3. Output voltage ripple is shown in figure 5.7. Voltage ripple under light load is not as bad, but under high load it is higher than expected. However, the power supply is still usable for this application.

U_{in} [V]	U_{out} [V]	I_{in} [A]	I_{out} [A]	P_{in} [W]	P_{out} [W]	η [%]
3.040	12.210	0.107	0.012	0.33	0.15	**45.8**
2.873	12.200	0.636	0.110	1.83	1.34	**73.4**

Table 5.3: 12V SMB Power Supply Test Results

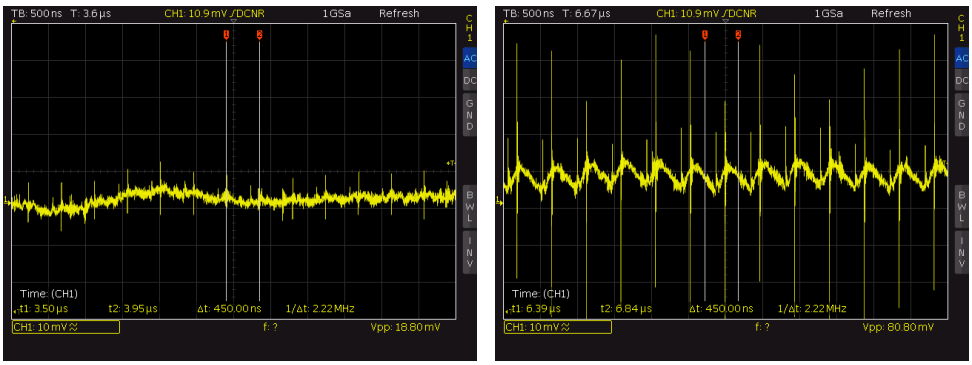

(a) : Minimal load **(b) :** High load

Figure 5.7: Output voltage ripple of 12V SMB power supply

Supercapacitor Charger

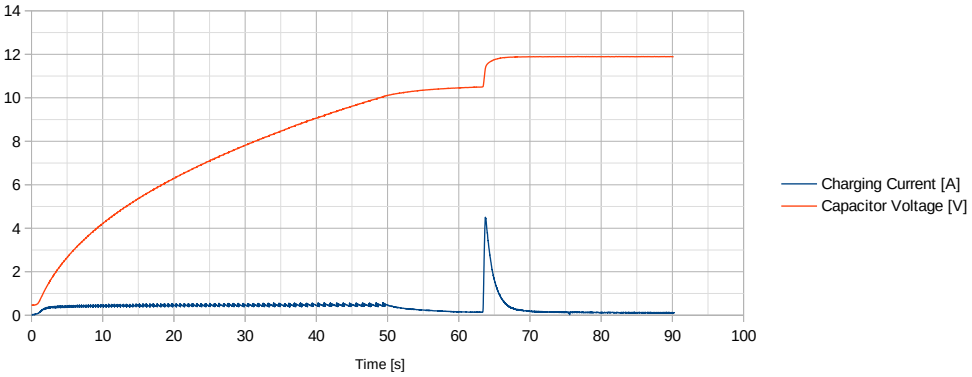

Figure 5.8: Supercapacitor charging process

Supercapacitor charging circuit was tested. The charger is controlled by a PI regulator implemented in the microcontroller firmware. In this case it regulates charging current to $0.5\,A$ until maximum duty cycle of the charger is reached $50\,s$ after start. Because the duty cycle cannot be increased any more, the charging current drops down. When supercapacitor voltage reaches $1.5\,V$ below the input voltage, the charger bypass is enabled. It slowly ramps up output voltage to limit capacitor charging current. This behaves according to the calculations in section 4.3.1. After this process is complete, the supercapacitor stack is fully charged and connected to the RocketBus, providing a stable high current power source to the actuator outputs.

The supercapacitor stack can power the section management board for up to 5 minutes until the voltage drops from $12\,V$ to $5\,V$. This is long enough for a complete flight of the rocket with reserve for recovery system deployment.

Supercapacitor Charger Bypass

Inrush current control feature of the supercapacitor charger bypass was tested. Output voltage ramp is shown in figure 5.9 and is faster than calculated during the design phase, but it is still usable.

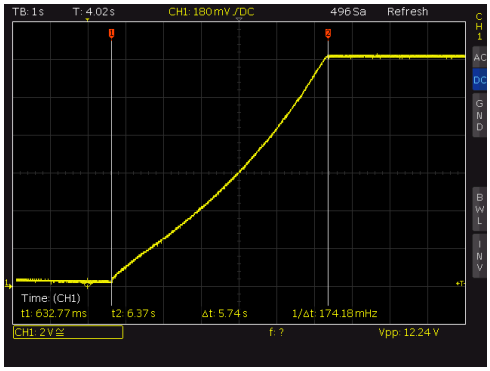

Figure 5.9: Inrush Current Control Voltage Ramp

Reverse Power Delivery

The reverse power delivery system was tested as shown in figure 5.10. During the test the supercapacitors were discharged through a 3.6 Ω resistor. The discharge process begins with current $I_d = 3.28\,A$ and gradually lowers as the supercapacitor voltage decreases. The output voltage and current drop slightly when undervoltage lockout is activated and the ideal diode is no longer ideal.

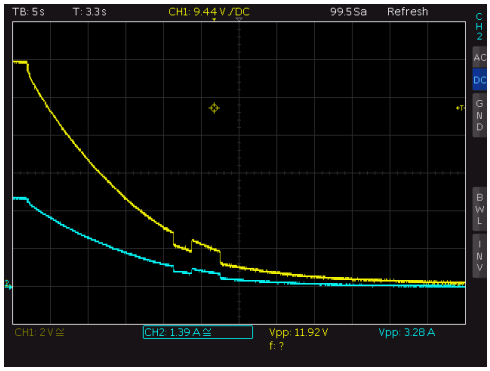

Figure 5.10: Reverse Power Delivery Test

5.2.2 Sensor Inputs

Measurement of sensor inputs characteristics was performed and the results are shown in figure 5.11. Measurement was done for current loop input in range of 0-25 mA. The input circuit behaves well without any distortion of input signal. A slight gain error was observed but that can be easily corrected

with calibration. Maximum deviation from ideal characteristics was 0.41% FS before calibration.

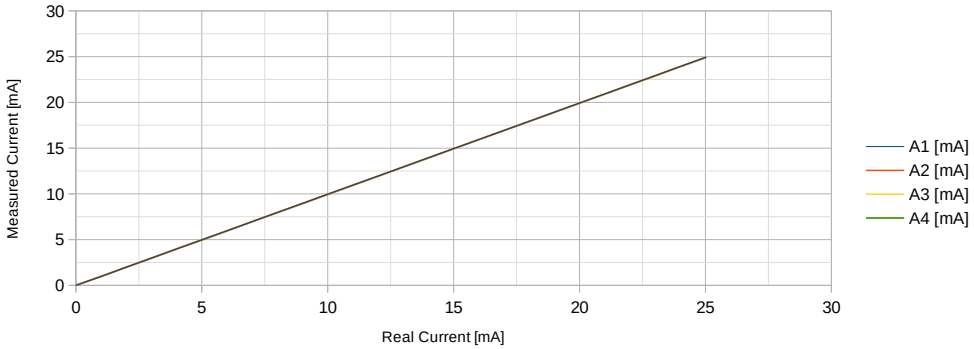

Figure 5.11: Sensor Input Transfer Characteristics

5.2.3 Actuator Outputs

Servo Outputs

Correct function of the servo signal driver was tested for serial bus communication using highest expected baudrate 1 $MBaud/s$. The measured communication waveform is shown in figure 5.12. Waveform of requests from the signal driver to the servo is good. Response from the servo is slightly deformed, however, correct data was received. Most probably, this is an issue of the communication circuit inside the servo. Overall, the servo signal driver circuit works correctly.

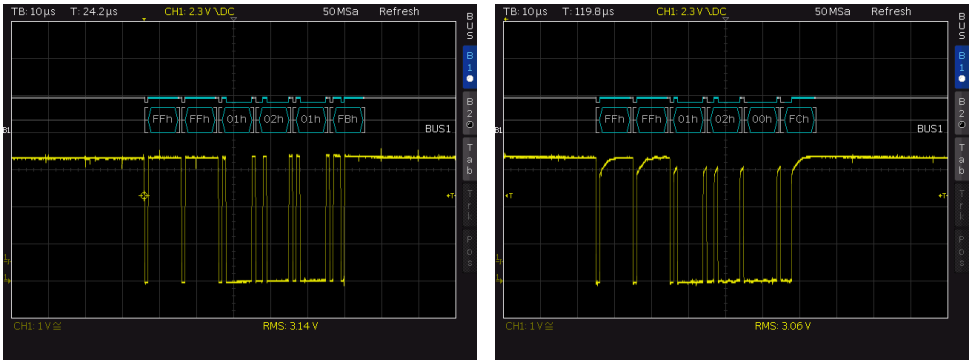

(a) : Servo Request **(b) :** Servo Response

Figure 5.12: Serial Bus Servo Communication Measurement

Power Outputs

Power outputs for actuators work correctly. No current is let through until nSLEEP input is set to high. The circuit was tested with 2 s long current pulses with amplitude 3.44 A as shown in figure 5.13 and the H-bridge was cold to touch even after prolonged period of pulsed output. A minor issue

with output state light indicator on the flight computer was encountered. The indicator LEDs are swapped and thus when output 1 is turned on, LED for output 2 lights up. This can be solved by rewriting silkscreen markings.

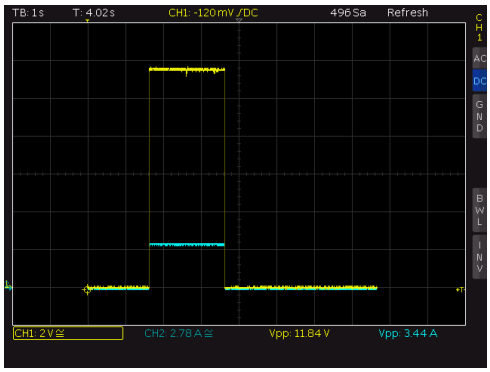

Figure 5.13: Actuator Power Output Test

Continuity Tester

Behaviour of continuity tester circuits was tested on both the flight computer and the section management board. Both continuity tester circuits are able to correctly detect connection of electronic match. When the electronic match is connected, the measured continuity detection voltage changes from $1.8\,V$ to $0.65\,V$ for the flight computer and from $0\,V$ to $0.88\,V$ for the section management board. This is large enough change to reliably confirm continuity of electronic match connection. Detection current flowing through the load was measured to be $1.2\,mA$ for the flight computer and $0.5\,mA$ for the section management board. This current is significantly lower then minimum ignition current of the electronic match and therefore is safe to use.

However, behaviour of the continuity detection circuits slightly differs from what is described by equations 3.30 and 4.24. It was observed that this is caused by the H-bridge as its output terminals sink some current to the ground. Measurement of current sink depending on voltage was done and based on that a model of the H-bridge was estimated as shown in figure 5.14. When the H-bridge is disabled, each of the output terminals can be approximated by a series connection of a diode and $1.5\,k\Omega$ resistor. In addition, a $12\,k\Omega$ resistor is connected between the output terminals. This needs to be taken into account when resistance of the load is to be estimated.

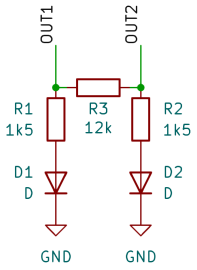

Figure 5.14: Estimated H-bridge Output Model for Continuity Tester

Chapter 6

Conclusion

Universal avionics platform is proposed in this thesis. The design is focused on versatility to allow control of complex high-power rockets equipped with hybrid or liquid fuel engines as well as smaller model rockets. This goal was achieved using modular design that can be modified to suit the needs of the rocket. Safety of the whole system is an important issue and was discussed as well. The arming and disarming procedure is described.

Besides the avionics platform itself, the most critical parts of the system are designed in this thesis according to requirements set by CTU Space Research team. The flight computer and section management board were designed, manufactured and tested. The flight computer is controlled by a microcontroller that can run team's existing flight software as well as the PX4 real-time operating system. Basic set of sensors for flight control is integrated into the flight computer as well as a microSD card for flight data logging. Wireless telemetry transceiver module is used for communication with the ground station. CAN bus is used for communication between all parts of the avionics platform. Section management board is responsible for control of all actuators and sensors in more complex rockets. It is equipped with supercapacitors to help deliver high-current pulses that might be required by the actuators. The supercapacitor stack acts also as a backup power supply in case of main power failure.

Both boards have been manufactured and tested. The 3.3V switching power supply present on both boards works well. The 12V power supply on the section management board produces higher voltage ripple then expected, but it is still usable. External sensor input circuits were tested and their transfer characteristics closely match the ideal one. Universal servo output circuit behaves according to design expectations. Continuity tester circuit for actuator power outputs has been tested as well and can be used for reliable continuity detection, however, it deviates from designed characteristics, because it is affected by the H-bridge integrated circuit.

In future, more thorough testing will be performed when the control software is ready. The avionics system will be stress-tested to confirm correct operation under high intensity vibrations or other environmental conditions. In the end, the avionics platform will be integrated into a rocket to be used at a rocketry competition.

Bibliography

[1] Electric match. In: *Wikipedia: the free encyclopedia* [online]. San Francisco (CA): Wikimedia Foundation [cit. 2024-05-24]. URL: https://en.wikipedia.org/wiki/Electric_match

[2] Rocket candy. In: *Wikipedia: the free encyclopedia* [online]. San Francisco (CA): Wikimedia Foundation [cit. 2024-05-24]. URL: https://en.wikipedia.org/wiki/Rocket_candy

[3] *PX4 Autopilot User Guide* [online]. [cit. 2024-05-24]. URL: https://docs.px4.io/main/en/

[4] *CATS Vega* [online]. [cit. 2024-05-24]. URL: https://www.catsystems.io/vega

[5] *Signal R2 TVC Kit - BPS.Space* [online]. [cit. 2024-05-24]. URL: https://bps.space/products/signal-r2

[6] *Eggtimer Altimeter Comparison* [online]. [cit. 2024-05-24]. URL: http://eggtimerrocketry.com/wp-content/uploads/2023/08/Eggtimer-Altimeter-Comparison-2023-08.pdf

[7] ZAPADLO, Aleš. *Flight Computer for Small Rocket*. Prague, 2023. Bachelor-s thesis. Czech Technical University in Prague, Faculty of Electrical Engineering, Department of Radioelectronic.

[8] *Silicdyne Fluctus Documentation and User Manual* [online]. 2024 [cit. 2024-05-24]. URL: http://silicdyne.net/fluctusdoc

[9] *Introduction to the Controller Area Network (CAN)* [online]. 2002, 2016 [cit. 2024-05-24]. URL: https://www.ti.com/lit/an/sloa101b/sloa101b.pdf

[10] *Ultra-Fit Power Connectors 3.50mm Pitch Datasheet* [online]. 2022 [cit. 2024-05-24]. URL: https://www.molex.com/content/dam/molex/molex-dot-com/en_us/pdf/datasheets/987651-1008.pdf?inline

[11] *KKPlus Connector System Product Family Datasheet* [online]. 2022 [cit. 2024-05-24]. URL: https://www.molex.com/content/dam/molex/molex-dot-com/en_us/pdf/datasheets/987651-9951.pdf?inline

[12] *Irradiation Cross-Linking of Polymers for Wire and Cable* [online]. [cit. 2024-05-24]. URL: https://www.champcable.com/wp-content/uploads/2019/01/Irradiation-Cross-Linking-of-Polymers-Short.pdf

[13] *PROCESS-CONTROLLED WIRE AND CABLE, RADIATION-CROSSLINKED, MODIFIED ETFE*-INSULATED Specification* [online]. 2015 [cit. 2024-05-24]. URL: https://www.te.com/commerce/DocumentDelivery/DDEController?Action=showdoc&DocId=Specification+Or+Standard%7FSPEC55PC%7F8%7Fpdf%7FEnglish%7FENG_SS_SPEC55PC_8.pdf

[14] WANG, Wen-Shin. *Can Automotive-qualified ICs Be Used in Industrial Applications?* [online]. 2016 [cit. 2024-05-24]. URL: https://www.ti.com/lit/ta/ssztbe8/ssztbe8.pdf

[15] *Pixhawk Standard Autopilots* [online]. [cit. 2024-05-24]. URL: https://docs.px4.io/main/en/flight_controller/autopilot_pixhawk_standard.html

[16] *STMicroelectronics STM32 Hardware Support from Simulink* [online]. [cit. 2024-05-24]. URL: https://www.mathworks.com/hardware-support/stm32.html

[17] *NuttX ST STM32H7 Supported MCUs* [online]. 2023 [cit. 2024-05-24]. URL: https://nuttx.apache.org/docs/latest/platforms/arm/stm32h7/index.html

[18] *STM32H742xI/G STM32H743xI/G Datasheet* [online]. 2023 [cit. 2024-05-24]. URL: https://www.st.com/resource/en/datasheet/stm32h743vi.pdf

[19] *Guidelines for oscillator design on STM8AF/AL/S and STM32 MCUs/MPUs* [online]. 2024 [cit. 2024-05-24]. URL: https://www.st.com/resource/en/application_note/an2867-guidelines-for-oscillator-design-on-stm8afals-and-stm32-mcusmpus-stmicroelectronics.pdf

[20] MUTTER, Arthur. Robustness of a CAN FD Bus System - About Oscillator Tolerance and Edge Deviations. *IEEE iCC* [online]. 2013, 8 [cit. 2024-05-24]. URL: https://www.bosch-semiconductors.com/media/ip_modules/pdf_2/papers/icc14_2013_paper_mutter_1.pdf

[21] *I2C Bus Pullup Resistor Calculation* [online]. 2015 [cit. 2024-05-24]. URL: https://www.ti.com/lit/an/slva689/slva689.pdf

[22] *Pressure Altitude Calculations* [online]. [cit. 2024-05-24]. URL: https://www.weather.gov/media/epz/wxcalc/pressureAltitude.pdf

[23] *BMP585 Barometric Pressure Sensor Datasheet* [online]. 2024 [cit. 2024-05-24]. URL: https://www.bosch-sensortec.com/media/boschsensortec/downloads/datasheets/bst-bmp585-ds003.pdf

[24] *ISM330DHCX Datasheet* [online]. 2020 [cit. 2024-05-24]. URL: https://www.st.com/resource/en/datasheet/ism330dhcx.pdf

[25] *MMC5983MA Datasheet* [online]. 2019 [cit. 2024-05-24]. URL: https://www.memsic.com/Public/Uploads/uploadfile/files/20220119/MMC5983MADatasheetRevA.pdf

[26] *SAM-M10Q Datasheet* [online]. 2022, 2024 [cit. 2024-05-24]. URL: https://content.u-blox.com/sites/default/files/documents/SAM-M10Q_DataSheet_UBX-22013293.pdf

[27] *POLYFUSE PTC SELECTION GUIDE* [online]. 2006 [cit. 2024-05-24]. URL: https://m.littelfuse.com/~/media/electronics_technical/application_notes/resettable_ptcs/littelfuse_polyfuse_ptc_selection_guide_application_note.pdf

[28] *TPS25981x Datasheet* [online]. 2022, 2023 [cit. 2024-05-24]. URL: https://www.ti.com/lit/ds/symlink/tps25981.pdf

[29] *V1PL45 Datasheet* [online]. 2020 [cit. 2024-05-24]. URL: https://www.vishay.com/docs/87642/v1pl45.pdf

[30] *LMR436x0-Q1 Datasheet* [online]. 2020, 2024 [cit. 2024-05-24]. URL: https://www.ti.com/lit/ds/symlink/lmr43620-q1.pdf

[31] HAUKE, Brigitte. *Basic Calculation of a Buck Converter's Power Stage* [online]. 2011, 2015 [cit. 2024-05-24]. URL: https://www.ti.com/lit/an/slva477b/slva477b.pdf

[32] *VCC: Capacitance Change vs Voltage in Ceramic Capacitors* [online]. [cit. 2024-05-24]. URL: https://www.digikey.com/Site/Global/Layouts/DownloadPdf.ashx?pdfUrl=863968494F2E4E13BBEA65B55A358443

[33] *AP7370 Datasheet* [online]. 2019 [cit. 2024-05-24]. URL: https://www.diodes.com/assets/Datasheets/products_inactive_data/AP7370.pdf

[34] WAVESHARE. *Bus servo control circuit* [online]. 2022 [cit. 2024-05-24]. URL: https://www.waveshare.com/w/upload/d/d3/Bus_servo_control_circuit.pdf

[35] *Hiwonder Bus Servo Communication Protocol* [online]. [cit. 2024-05-24]. URL: https://drive.google.com/file/d/ 12tG-gHq0zagPBs6z3pYk4KPHAeVgfbiTW/view

[36] *SBUS2-Telemetry* [online]. 2020 [cit. 2024-05-24]. URL: https://github.com/BrushlessPower/SBUS2-Telemetry

[37] *DRV8256E/P Datasheet* [online]. 2020 [cit. 2024-05-24]. URL: https://www.ti.com/lit/ds/symlink/drv8256.pdf

[38] ZÁHLAVA, Vít. *Návrh a konstrukce desek plošných spojů: principy a pravidla praktického návrhu*. Praha: BEN - technická literatura, 2010. ISBN 978-80-7300-266-4.

[39] *Overview of USB Type-C and Power Delivery technologies* [online]. 2018 [cit. 2024-05-24]. URL: https://www.st.com/resource/en/technical_article/ta0357-overview-of-usb-typec-and-power-delivery-technologies-stmicroelectronics.pdf

[40] *STM32F746G-DISCO Schematics* [online]. 2022 [cit. 2024-05-24]. URL: https://www.st.com/resource/en/schematic_pack/mb1191-f746ngh6-c03-schematic.pdf

[41] *CMT-8504-100-SMT-TR Datasheet* [online]. 2022 [cit. 2024-05-24]. URL: https://www.cuidevices.com/product/resource/pdf/cmt-8504-100-smt-tr.pdf

[42] *STM32G491xC STM32G491xE Datasheet* [online]. 2024 [cit. 2024-05-24]. URL: https://www.st.com/resource/en/datasheet/stm32g491me.pdf

[43] VOBECKÝ, Jan a Vít ZÁHLAVA. *Elektronika: Součástky a obvody, principy a příklady*. 3. rozš. vydání. Grada Publishing, 2005. ISBN 978-80-247-1241-3.

[44] FALIN, Jeff. *How to Quickly and Safely Charge Supercapacitors* [online]. 2023 [cit. 2024-05-24]. URL: https://www.ti.com/lit/an/sluaao7/sluaao7.pdf

[45] *ADP3120A Datasheet* [online]. 2018 [cit. 2024-05-24]. URL: https://www.onsemi.com/download/data-sheet/pdf/adp3120a-d.pdf

[46] *SSM6K504NU Datasheet* [online]. 2012, 2023 [cit. 2024-05-24]. URL: https://toshiba.semicon-storage.com/info/SSM6K504NU_datasheet_en_20230118.pdf?did=13720&prodName=SSM6K504NU

[47] *LTC4451 Datasheet* [online]. 2021 [cit. 2024-05-24]. URL: https://www.analog.com/media/en/technical-documentation/data-sheets/ltc4451.pdf

[48] *TPS25983 Datasheet* [online]. 2023 [cit. 2024-05-24]. URL: https://www.ti.com/lit/ds/symlink/tps25983.pdf

[49] *TPS61379 Calculation Tool v1.0* [online]. 2024 [cit. 2024-05-24]. URL: https://www.ti.com/tool/download/SLVRBI0

[50] PAONESSA, Simon a Bruce MCDUFFEE. *Back To Basics: The Fundamentals of 4-20 mA Current Loops* [online]. [cit. 2024-05-24]. URL: https://www.predig.com/sites/default/files/documents/whitepapers/4-20_mA_Current_Loop_Fundamentals.pdf

[51] *PT5300 Pressure transmitter datasheet* [online]. 2023 [cit. 2024-05-24]. URL: https://www.ifm.com/restservices/cz/cs/assets/c3VwcGxpZXJzL2lmbS9kb2N1bWVudHMvcHJvZHVjdC9QVDUzMDAtMDEvZGF0ZW5ibGFldHRlci9QVDUzMDAtMDFfRU4tVVMucGRm

Appendix A

Attached DVD Content

All design files are provided alongside the thesis on the attached DVD. Circuit schematics and board designs for both boards are provided in form of KiCAD project files. In addition, exported schematics and board designs in PDF format are provided as well.

In root folder of the attached DVD, there are folders *Cimrman2*, *Zora2* and *Exports*. In folder *Cimrman2* there is the main project file *cimrman2.kicad_pro* for the flight computer. In folder *Zora2* there is the main project file *Zora2.kicad_pro* for the section management board. Folder *Exports* contains the exported schematics and board designs in PDF format.